NRL Memorandum Report 2101

ARPA Coupling Program on Stress-Corrosion Cracking (Thirteenth Quarterly Report)

G. SANDOZ
(General Editor)

Physical Metallurgy Branch
Metallurgy Division

Sponsored by

Advanced Research Projects Agency
ARPA Order No. 878

March 1970

NAVAL RESEARCH LABORATORY
Washington, D.C.

Quarterly Report Series on the

ARPA COUPLING PROGRAM ON STRESS-CORROSION CRACKING

First Quarterly Report, NRL Memorandum Report 1739 (Dec 1966)

Second Quarterly Report, NRL Memorandum Report 1775 (Apr 1967)

Third Quarterly Report, NRL Memorandum Report 1812 (Aug 1967)

Fourth Quarterly Report, NRL Memorandum Report 1834 (Nov 1967)

Fifth Quarterly Report, NRL Memorandum Report 1864 (Feb 1968)

Sixth Quarterly Report, NRL Memorandum Report 1902 (Jun 1968)

Seventh Quarterly Report, NRL Memorandum Report 1941 (Oct 1968)

Eighth Quarterly Report, NRL Memorandum Report 1965 (Jan 1969)

Ninth Quarterly Report, NRL Memorandum Report 1991 (Mar 1969)

Tenth Quarterly Report, NRL Memorandum Report 2013 (May 1969)

Eleventh Quarterly Report, NRL Memorandum Report 2028 (Jul 1969)

Twelfth Quarterly Report, NRL Memorandum Report 2060 (Oct 1969)

BLANK PAGE

CONTENTS

ABSTRACT

A progress report of the research investigations being carried out on the problem of stress-corrosion cracking of high strength materials under ARPA Order 878 is presented. Work at Carnegie-Mellon University, Lehigh University, Georgia Institute of Technology, The Boeing Company, American University, and the Naval Research Laboratory concerning test techniques, materials characterization, physical metallurgy, surface studies, and corrosion fatigue is described. The report is divided into three main sections covering work on high strength titanium, steel, and aluminum. Included is a section containing abstracts of recently published reports, journal articles, and talks generated under ARPA Order 878. Selected abstracts of articles from outside the ARPA program in the field of stress-corrosion cracking are also included as well as a Diary of Events section.

STATUS

This is a progress report; work is continuing.

AUTHORIZATION

NRL Problems 60M04-08
61M04-08
63M04-08A
ARPA Order 878 and
RR 007-08-44-5512

This research was supported by the Advanced Research Projects Agency of the Department of Defense, NRL Problem M04-08, and was monitored by the Naval Research Laboratory under Contract Nos. Nonr-610(09), Nonr-760(31), N00014-66-C0365, Nonr-991(15), N00014-68A-0245-0001, and N00014-68-A-0173-0003.

ARPA Coupling Program on Stress-Corrosion Cracking
(Thirteenth Quarterly Report)

INTRODUCTION

The problem area of stress-corrosion cracking (SCC) in structural materials leading to failures in engineering structures has been of continuing concern to the Department of Defense and to other users of structural materials. Although considerable progress had been made in the field of corrosion, insufficient information was available to reach reliable conclusions on the phenomena of SCC and on the mechanisms involved. Without the development of reliable mechanism(s) and understanding of the factors involved in SCC phenomena, development and application of high strength alloys for reliable service in various environments can proceed only empirically.

In order to bridge the gap in fundamental knowledge needed to understand and to cope with the problem of SCC and to apply this knowledge to obtaining improvement of SCC resistance in existing and newly developed high strength alloys, the Advanced Research Projects Agency (ARPA) of DoD established a project on SCC under ARPA Order 878. This project, a broadly based interdisciplinary experiment, involves a coupling program between academic, industrial, and Government laboratory participants. The technological goal is to learn how to improve high strength structural alloys with respect to their resistance to SCC under various environmental and stress conditions, or at least learn how to "live with" the alloys which we have not been able to improve sufficiently.

Academic disciplines needed in the attack on the SCC problem area were considered to include: modern physical metallurgy, surface chemistry and electrochemistry, physics of surfaces, continuum mechanics as applied to fracture, advanced techniques of analysis, and development of environment-metal reaction theory. The industrial participant affords a means of amplifying a Government laboratory's in-house capability without an increase in in-house staff. The Government laboratory's role was to exercise overall project direction, to provide direction guidance as to DoD needs, and to conduct basic and applied research.

The academic participants and their principal discipline areas include the following:

a. Carnegie-Mellon University -- Advanced physical metallurgy and electrochemistry.

b. Georgia Institute of Technology -- Surface physics and physical metallurgy.

c. Lehigh University -- Surface chemistry, metallurgy, and fracture mechanics.

d. American University -- Solution chemistry and electrochemical effects (in aluminum).

e. University of Florida -- Electrochemistry, particularly in conducting Pourbaix-type analyses for alloy systems.

The Boeing Company, the industrial partner, develops standard test methods and characterizes SCC properties of advanced high strength alloys; provides technical guidance in areas of special competence; and conducts a limited amount of basic research in related areas.

The Naval Research Laboratory is the Government laboratory participant. Its research and discipline areas are: physical metallurgy, electrochemistry, surface chemistry, solution chemistry, surface physics, and fracture mechanics.

In addition, NRL identifies relevant military hardware needs in the area of SCC.

The technical reporting system includes the following:

Detailed technical progress from each project participant is published twice yearly in the quarterly report series. The technical progress report is organized into three main categories: Titanium, Steel, Aluminum. Each main category is further divided according to material classification and to research discipline. The individual progress reports are sent to and edited by category editors who in turn submit the edited progress reports to NRL for assembly into the quarterly report and publication as an NRL report. The remaining two quarterly reports contain 1) abstracts of newly published reports of project sponsored research, 2) a chronological list of titles of all ARPA-generated reports, and 3) selected abstracts of reports and journal articles of work related to SCC outside the ARPA project. A final item is a diary of events section.

A. TITANIUM

Commercial Alloys

Physical Metallurgy

The effect of microstructure on the susceptibility to stress-corrosion cracking of the metastable beta Ti-11.5Mo-6Zr-4.5Sn (Beta III) has been studied at Boeing. In agreement with work on the alloy Ti-8Mn (1), as-quenched and omega-strengthened Beta III showed no environmental cracking in aqueous solutions containing halide ions. The beta plus alpha microstructures, however, were susceptible to stress-corrosion cracking, the degree of susceptibility being strongly dependent on the aging temperature, the environment, and the applied potential.

Fatigue precracked notched-bend specimens (7 in. by 1.5 in. by 0.625 in.) were deadweight loaded in cantilever bending using the technique described by Brown (2). The 3.5% NaCl solution was continually dripped into the specimen notch. The threshold level or K_{Iscc} for specimens aged at 900°F was 26 ksi $\sqrt{in}$. No failures were obtained in similar notched-bend specimens aged at 1150°F with K_{IQ} = 99 ksi $\sqrt{in}$.

Crack velocity versus stress-intensity factor (K) data obtained under controlled potentiostatic conditions on fatigue precracked single edge notched specimens (6 in. by 1 in. by 0.10 in.) aged at 900°F are shown in Fig. A-1. The halide solutions (0.6 M KCl and 5.0 M KI) and potentiostatic conditions used in this investigation have been demonstrated to be most severe for Ti-8Mn (1) and Ti-8Al-1Mo-1V (3). The results showed a plateau where the crack velocity is independent of stress intensity. This plateau has been observed in aluminum alloys (4) and has been termed region II. Although a constant average velocity is observed in region II, cracking was in fact discontinuous. The arrows drawn from the first data points parallel to the ordinate represent the initiation K for environmental growth (approximately K_{Iscc}) and where velocity goes to zero (1,4).

The iodide solution promotes a higher crack velocity and a lower initiation K ($\sim K_{Iscc}$) than the chloride solution. Also, under the more severe conditions of an applied potential, the K_{Iscc} for 0.6 M KCl is somewhat lower than the threshold level determined on similarly aged notched-bend specimens in 3.5% NaCl solution with no applied potential. Limited crack velocity data for specimens aged at 900°F and tested in distilled water are shown in

Fig. A-1 together with the identical K_{Ic} and K_{Iscc} values for omega-strengthened specimens aged at 700° F.

Stress-corrosion cracking data for specimens aged at 1150° F and tested under controlled potentiostatic conditions are shown in Fig. A-2. It can be seen that a marked degree of susceptibility is exhibited. However, the variation of crack velocity with stress intensity is different in each halide solution. In 0.6 M KCl, the variation of crack velocity with stress intensity is similar to that observed in specimens aged at 900° F; that is, region II is exhibited. However, in 5.0 M KI there is no region where crack velocity is independent of K. The initiation stress intensity in 5.0 M KI is significantly affected by strain rate (or crosshead displacement rate), failure occurring immediately after initiation at a crosshead displacement rate of 0.1 cm/min. It is not surprising, therefore, that environmental influences were absent in the "static" notched-bend tests.

The fracture mode in 3.5% NaCl, 0.6 M KCl, and 5.0 M KI is intergranular. This result contrasts with other observations in both alpha phase (5) and beta phase (1,4,6) titanium alloys where stress-corrosion cracking in aqueous solutions has been shown to be associated with a transgranular mode of failure.

The influence of "orientation" (defined as the relationship between preferred basal plane orientation and specimen orientation) on the stress-corrosion susceptibility of Ti-8Al-1Mo-1V alloy under near plane stress conditions has been determined at Boeing. Plane stress conditions were approached by varying (a) specimen thickness, (b) "orientation," and (c) yield strength of the alloy (by heat treatment). Susceptibility to stress-corrosion cracking was measured as a function of these variables by sustain loading single edge notched specimens in tension or in bending in aqueous 3.5% NaCl solution.

It was found that the expected tendency to approach plane stress conditions in the alloy by decreasing specimen thickness was dependent upon certain "orientations." Variations in yield strength and these "orientations," respectively, significantly influenced the susceptibility of thin specimens (0.02-in. thickness) to stress-corrosion cracking. These factors had only a minor effect on the susceptibility of thick specimens (0.4-in. thickness) where the plane strain stress state was predominant.

Whether corrodent was added to the specimen before or after loading significantly affected only the stress-

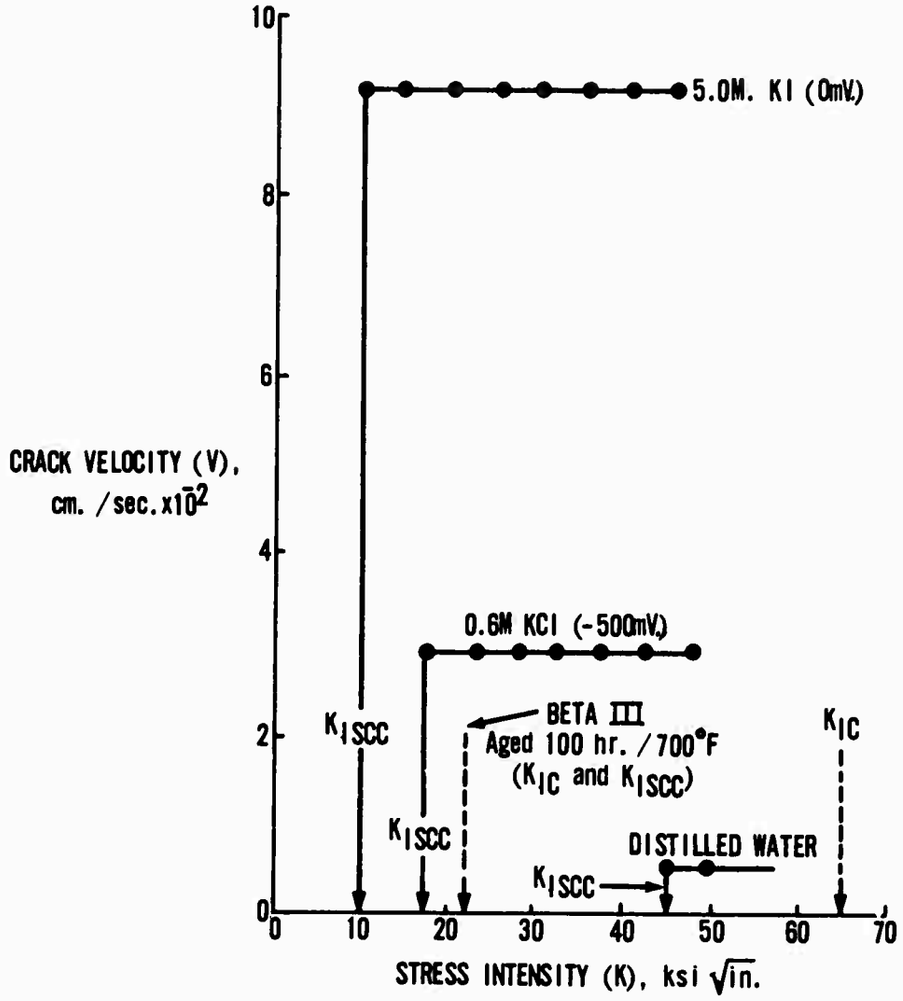

Fig. A-1 - Variation of crack velocity with stress intensity in 0.6 M KC1 and 5.0 M KI under controlled potentiostatic conditions for specimens of Ti-11.5Mo-6Zr-4.5Sn (Beta III) Aged 100 hours at 900°F. K_{Ic} and distilled water data are also included.

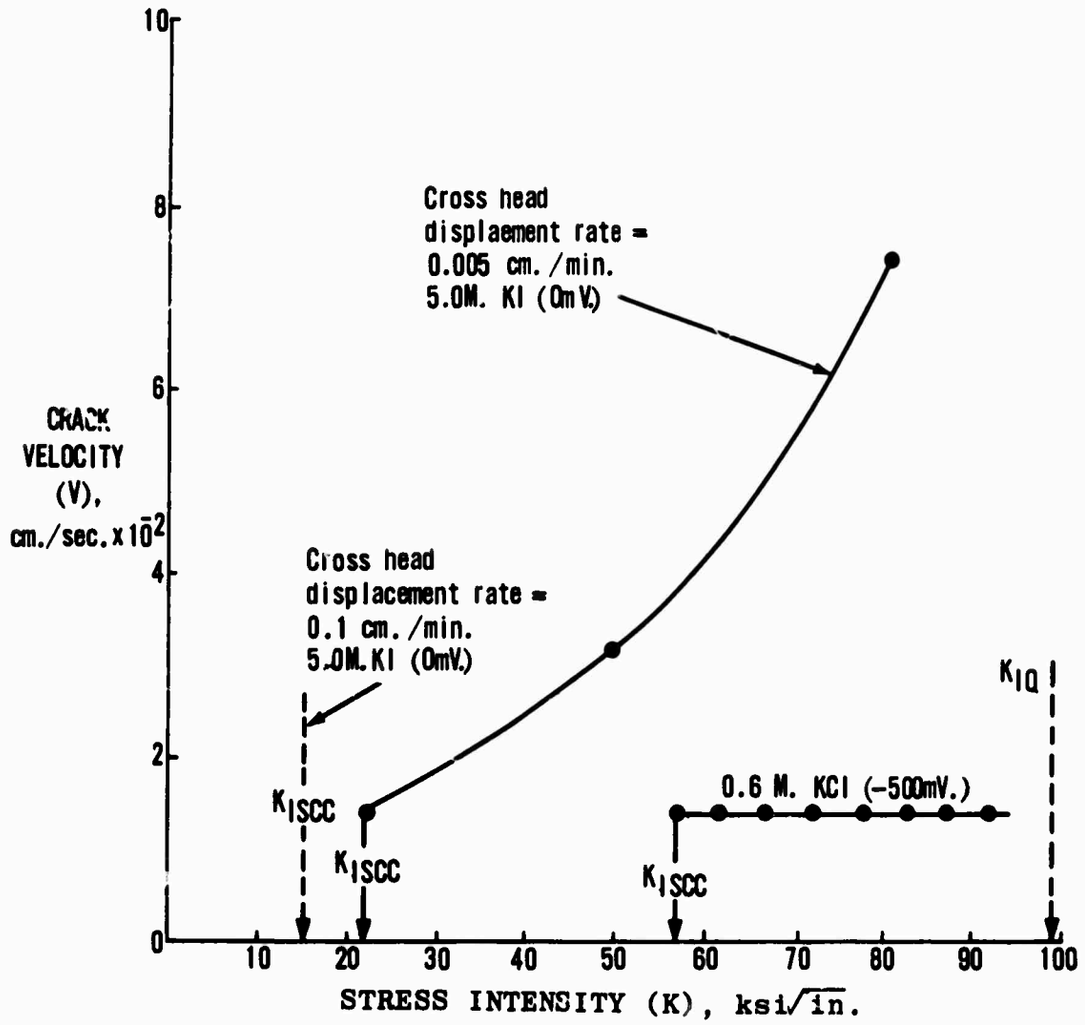

Fig. A-2 - Variation of crack velocity with stress intensity in 0.6 M KC1 and 5.0 M KI under controlled potentiostatic conditions for specimens of Ti-11.5Mo-6Zr-4.5Sn (Beta III) Aged 16 hours at 1150°F.

corrosion susceptibility of thin specimens. Specimens loaded prior to the addition of corrodent exhibited a much lower measured susceptibility than those stressed in the presence of the corrodent. This effect was independent of "orientation" and was not observed in thick specimens of Ti-8Al-1Mo-1V.

References

1. T. R. Beck and J. J. Blackburn, Quarterly Progress Report No. 7, NASA Contract NAS 7-489, March 1968.

2. B. F. Brown, ASTM Materials Research and Standards (1966), 66, p. 129.

3. T. R. Beck, "Stress Corrosion Cracking of Titanium Alloys, 1. Ti:8-1-1 Alloy in Aqueous Solutions," Journal of Electrochemical Society, vol. 114, 1967, p. 551.

4. T. R. Beck, M. J. Blackburn and M. O. Speidel, Quarterly Progress Report No. 11, NASA Contract NAS 7-489, March 1969.

5. E.g., Proceedings of Conference "Fundamental Aspects of Stress Corrosion Cracking," Ohio State University, R. W. Staehle, editor, NACE (1969).

6. D. N. Fager and W. F. Spurr, Trans. ASM (1968) 61, p. 283.

Addendum

At Georgia Tech, polarization curves for titanium-aluminum alloys containing approximately 2.5, 5, and 8% aluminum have been evaluated under static loads just below and above the yield point of the material. 3.5% NaCl solutions varying from pH 1.5 to 7 were used. The total corrosion current at the potential of maximum corrosion is relatively low for the unstressed materials or those stressed just below the yield point. In fact there is remarkably little difference in stress and stressed condition of all the alloys until the yield point, then a large increase in current and a shift towards the anodic potential is observed.

B. STEEL

COMMERCIAL ALLOYS

Characterization and Test Techniques

The effect of specimen thickness on the stress corrosion susceptibility of AISI 4340 steel has been studied at the Boeing Company. An 1-inch-thick plate of AISI 4340 steel was heat treated to an ultimate tensile strength level of 215 ksi, (yield strength - 192 ksi). The plane-strain fracture toughness, K_{Ic}, for the steel was found to be 69 ksi $\sqrt{in.}$, and the stress-corrosion threshold (for plane-strain), K_{Iscc}, 25 ksi $\sqrt{in.}$ The plate was machined to provide single-edge-notched specimens with thicknesses varying from 0.005 to 1.0 inch. Specimens with thicknesses equal to or exceeding 1/8 in. were tested in bending, whereas tension loading was used for the thinner specimens. To determine the stress-corrosion-threshold K_{scc}, 5 specimens for each thickness were tested under sustained loads, (corresponding to different initial stress intensity levels), in 3.5% aqueous sodium chloride solution. Higher K_{scc} was observed for the thinner specimens. The minimum value of K_{scc}, (corresponding to K_{Iscc}), was obtained when the specimen thickness was equal to or greater than $2.5(K_{Iscc}/F_{ty})^2$, where F_{ty} is the tensile yield strength.

In another study at Boeing, the influence of preloading on the stress-corrosion-cracking resistance of two ultrahigh-strength steels is being investigated. Fatigue pre-cracked, single-edge-notched specimens of an AISI 4340 steel (heat treated to a yield strength of 194 ksi) and a 300-grade 18Ni maraging steel are used. Work on the AISI 4340 steel has been completed, and tests on the maraging steel are in progress. The AISI 4340 steel specimens were preloaded in three-point bending in air to various stress-intensity levels, up to 90% of the K_{Ic} of 72 ksi $\sqrt{in.}$ After unloading, the effective stress-corrosion-cracking threshold K^*_{Iscc} was determined for each preload condition by testing the specimens in 3.5% aqueous sodium chloride solution under sustained-load cantilever bending. It was found that K^*_{Iscc} increased from 8 ksi $\sqrt{in.}$ (with no preloading) to greater than 25 ksi$\sqrt{in.}$, in proportion to the preload stress-intensity level, (Fig. B-1). The time-to-failure at applied stress intensity (K_{Ii}) levels above K^*_{Iscc} was not affected by the amount of preloading. The increase in the effective stress-corrosion-cracking threshold has been tentatively attributed to compressive stresses at the crack tip resulting from preloading. Preliminary results on the maraging steel indicate that preloading has little effect on the stress-corrosion-cracking threshold for this steel.

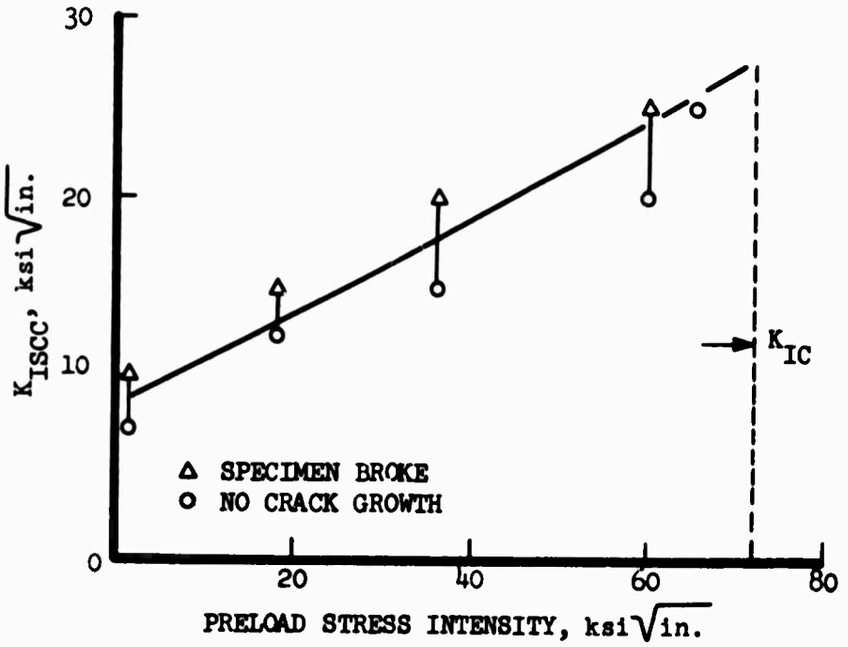

Fig. B-1 - Effect of preloading on the effective stress-corrosion-cracking threshold K^{*}_{Iscc} of AISI 4340 steel.

In a previous report (1), a simple, quantitative method, developed at Lehigh University, for estimating the effects of aggressive environments on fatigue-crack growth was discussed. This method suggests that the rate of fatigue-crack growth in an aggressive environment is equal to the algebraic sum of the rate of fatigue-crack growth in an inert reference environment and an environmental component, to be computed from the load profile and sustained-load crack-growth data, as a first order approximation. A more detailed discussion of this method has been reported elsewhere (2). Comparisons with available data at the time indicated that this superposition method correctly predicts the effect of test frequency. However, only qualitative agreement for the effect of stress ratio was noted. Recent experimental results obtained at Lehigh show that the effect of stress ratio is also accounted for correctly by this method. These results suggest that the sustained-load crack-growth-rates for AISI 4340 steel in distilled water, reported by Van der Sluys (3) and Gallagher (4), may be too high. Further verification are in progress.

Surface Studies

In the past several years, intergranular failures of high strength cadmium plated AISI 4340 steels have been examined at Georgia Tech. Hydrogen brittlement has always been deduced as the cause of failure based on fractographic results. The lack of an adequate bake after plating was usually blamed, but the possible relationship of the cadmium plating to stress corrosion was never adequately assessed. It is interesting to note that in reviewing the literature, the major reason cited

1. ARPA Coupling Program on Stress-Corrosion Cracking (Eleventh Quarterly Report), NRL Memorandum Report 2028, July 1969, pp. 5 and 20.

2. R. P. Wei and J. D. Landes, "Correlation between Sustained-Load and Fatigue Crack Growth in High-Strength Steels," Materials Research and Standards, Vol. 9, No. 7, 1969, p. 25.

3. A. W. Van der Sluys, "Mechanics of Environment Induced Subcritical Flaw Growth in AISI 4340 Steel," Transactions, Am. Soc. Mechanical Engrs., Ser. D, Vol. 89, 1967, p. 28.

4. J. P. Gallagher, "Environmentally Assisted Fatigue Crack Growth in SAE 4340 Steel," Ph.D. Dissertation, Dept. of Theoretical and Applied Mechanics, University of Illinois, Urbana, Illinois, 1968.

for cadmium plating was the improvement in the overall corrosion resistance. There has been very little consideration of any galvanic corrosion or stress corrosion effects due to the cadmium plating of high strength steels.

To evaluate the possible role of cadmium plating, four series of single-edge-notched bend specimens (1/2 in.by 5/8 in. by 6 in.) were prepared from an AISI 4340 steel heat-treated to a tensile strength level of 260 ksi. The series consisted of specimens that were 1) as-heat-treated, 2) cadmium plated, 3) cadmium plated plus a 24 hour hydrogen bake at 375° to 400°C, and 4) cadmium plated, baked and then the bottom of the notch scribed to remove the plating. The specimens were tested in a 3.5% NaCl solution. A bend stress at the base of the notch, calculated to be roughly 80% of the yield strength, was used for all specimens tested. Although this varied slightly from specimen to specimen, depending upon the actual radius at the root of the notch, results were fairly consistent. In the case of series 1 and 3 no breaking for nominal exposure to static stress was observed except one specimen which had gone through the cadmium plating and the 24 hour bake. For the cadmium plated and no baking series (series 2), all specimens failed in a very short period of time, some as short as 12 minutes. In the 4th series, specimens which were cadmium plated, baked and then the cadmium scribed away from the bottom of the notch followed by exposure to 3.5% NaCl solutions, broke in a very short period of time, some samples in less than 15 minutes. The fracture surface was studied and although the crack growth at the tip of the corroded samples was small it was still found to be typical of intergranular fracture observed in hydrogen embrittlement and stress-corrosion cracking (SCC) of high strength steels.

In further studies, the open circuit potential between cadmium plated material and "straight" AISI 4340 steel in the 260 ksi tensile strength range (or base material) was measured and found to be 270 millivolts. This polarized to 150 millivolts after an hour and a half but then remained essentially constant. In each case the base material was the cathode. Further studies to determine the actual electrode reactions are now under way, although one might assume from the evidence of the type of fracture that hydrogen evolved at the crack tip is absorbed at the notch during the corrosion process. Our analysis of the electrochemical data should prove or disprove this.

Although these studies are still in the early stages, the importance of the galvanic reaction between high strength AISI 4340 steel and cadmium plated surface cannot be completely neglected.

Initial experiments to determine the effects of oxide films on stress-corrosion cracking of AISI 4340 steel have been performed at the Naval Research Laboratory using U-bend specimens (1). Oxide films were produced by immersing the specimens in hot 50 percent caustic solution under anaerobic conditions using KNO_3 as the oxidizing agent. This procedure produced what appeared to be high integrity adherent coatings of Fe_3O_4 of 0.1 to 0.2 microns in thickness. By adding $MnSO_4$ to this solution a non-conductive film of $MnFe_2O_4$ could also be formed with good visual appearance.

These U-bend specimens were not capable of resolving any difference between the two coatings, but it became apparent that careful standardization of specimen preparation will be essential. Times to failure did not agree between duplicate specimens, and there was no correlation between bare iron plated specimens and oxide coated specimens. It is known from other work that oxide film grown from an overly strong caustic solution tends to form a film of greater porosity. Both types of these specimens appeared to corrode at the same rate in the 3.5% NaCl test solution. This may have masked the expected effect of oxide conductivity.

Visual determination of the presence of cracks, and even of whether the specimen was broken in some cases, was found to be unsatisfactory. Strain gages will be utilized in future tests.

Since it was believed important to avoid the possibility of charging the specimens with hydrogen either by pickling before plating or by the use of ordinary plating baths, neither of these procedures was used. However, since mechanical cleaning methods appear to be unsatisfactory from these first experiments, pickling will have to be used. Specimens will then be baked in a vacuum (below their tempering temperature) to remove hydrogen. Measures will be taken also to generate oxides of lower porosity; an available technique will be used to measure the relative porosities of different films.

---

1. ARPA Coupling Program on Stress Corrosion Cracking (Eleventh Quarterly Report), NRL Memorandum Report 2028, July 1969, pp. 23-24.

Stress-corrosion cracking of AISI 4340 steel is prevented by many inorganic and some organic compounds that inhibit general corrosion of this alloy. Higher concentrations of inhibitor are frequently required for prevention of SCC than are necessary to control general corrosion.

SIMPLIFIED EXPERIMENTAL PROJECT ALLOYS

Physical Metallurgy

The effects of alloying elements on the stress-corrosion-cracking threshold (K_{Iscc}) of laboratory-produced research (martensitic) steels, (similar to AISI 4340 steel in base composition), quenched and tempered to about 200 ksi yield strength continue to be studied at the Naval Research Laboratory. It was reported previously (1) that C and Mn lower K_{Iscc} severely. Additional studies have been conducted on new heats of steels to confirm these results, to extend the ranges of composition studied, and to determine the effects at a lower yield strength level.

The results for Mn are given in Figs. B-2 and B-3, for the steels at the 169 ksi and 187 ksi yield strength levels, respectively. Both series generally confirm that increasing amounts of Mn lower K_{Iscc}. At the 187 ksi yield strength level, however, there is a jog on the curve at about 0.5 percent Mn, a range of Mn not previously studied. No explanation for this jog could be found other than the speculation that desulfurizing or deoxidation reactions become maximized at about this Mn level. These effects, however, should also be observed at the 169 ksi yield strength level, where only a very slight jog can be visualized (Fig. B-2).

The results for carbon are given for Figs. B-4 and B-5 for the 172 ksi and 195 ksi yield strength ranges, respectively. Increasing carbon from 0.15 to about 0,4 percent reduces K_{Iscc}. This agrees with the previously reported results. Both K_{Ix} and K_{Iscc} values are generally higher in the lower yield strength (172 ksi) series as compared to the higher yield strength series, as expected. A rise in K_{Iscc} as the carbon content exceeds about 0.4 percent was reported previously (1), and the new series shows a similar effect. Another series of steels has now been

(1) ARPA Coupling Program on Stress Corrosion Cracking (Eleventh Quarterly Report), NRL Memorandum Report 2028, July 1969, p. 25.

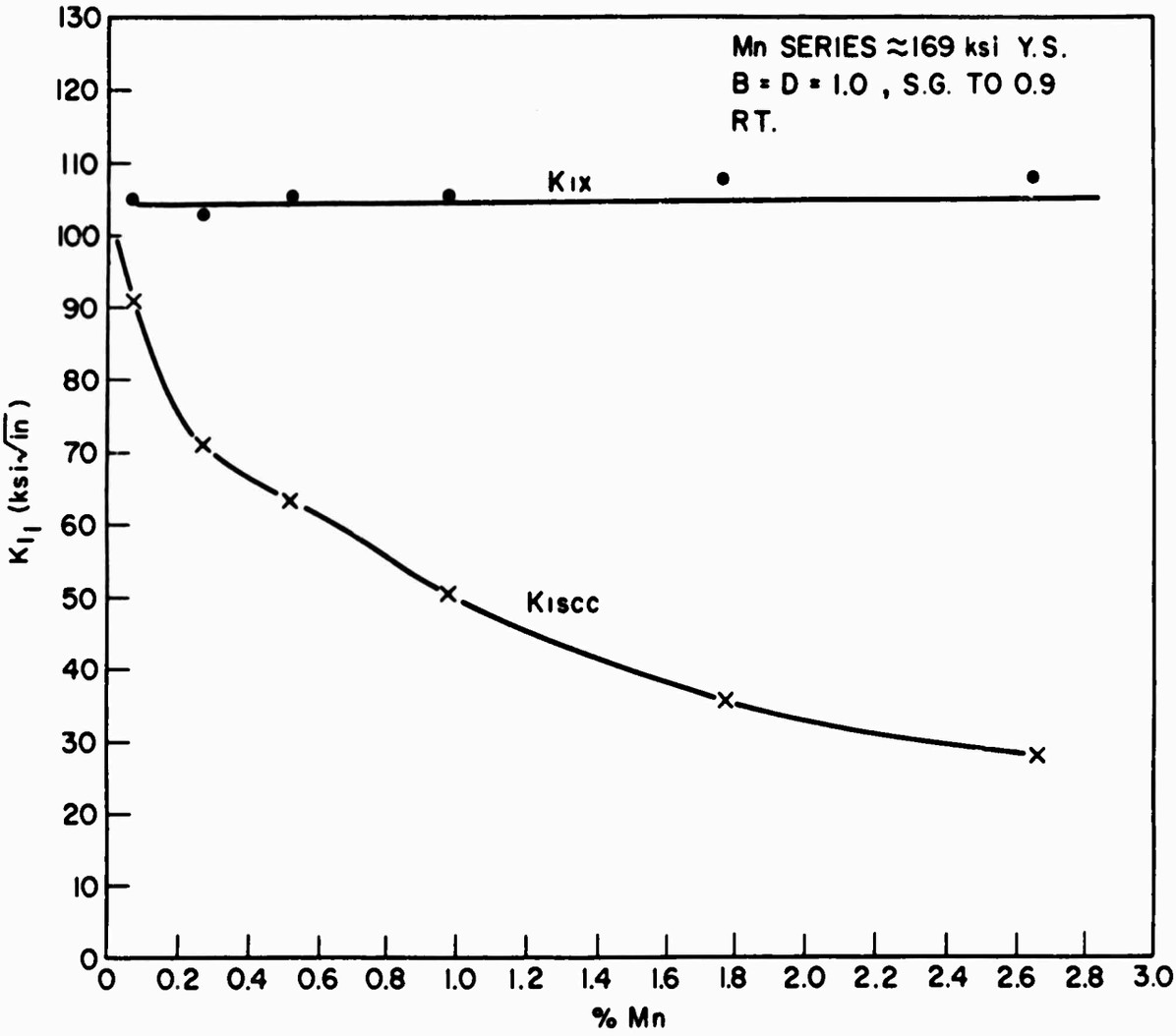

Fig. B-2 - Effects of Mn on the stress-corrosion-cracking resistance of steel similar to AISI 4340 in base composition and quenched and tempered to 169 ksi yield strength.

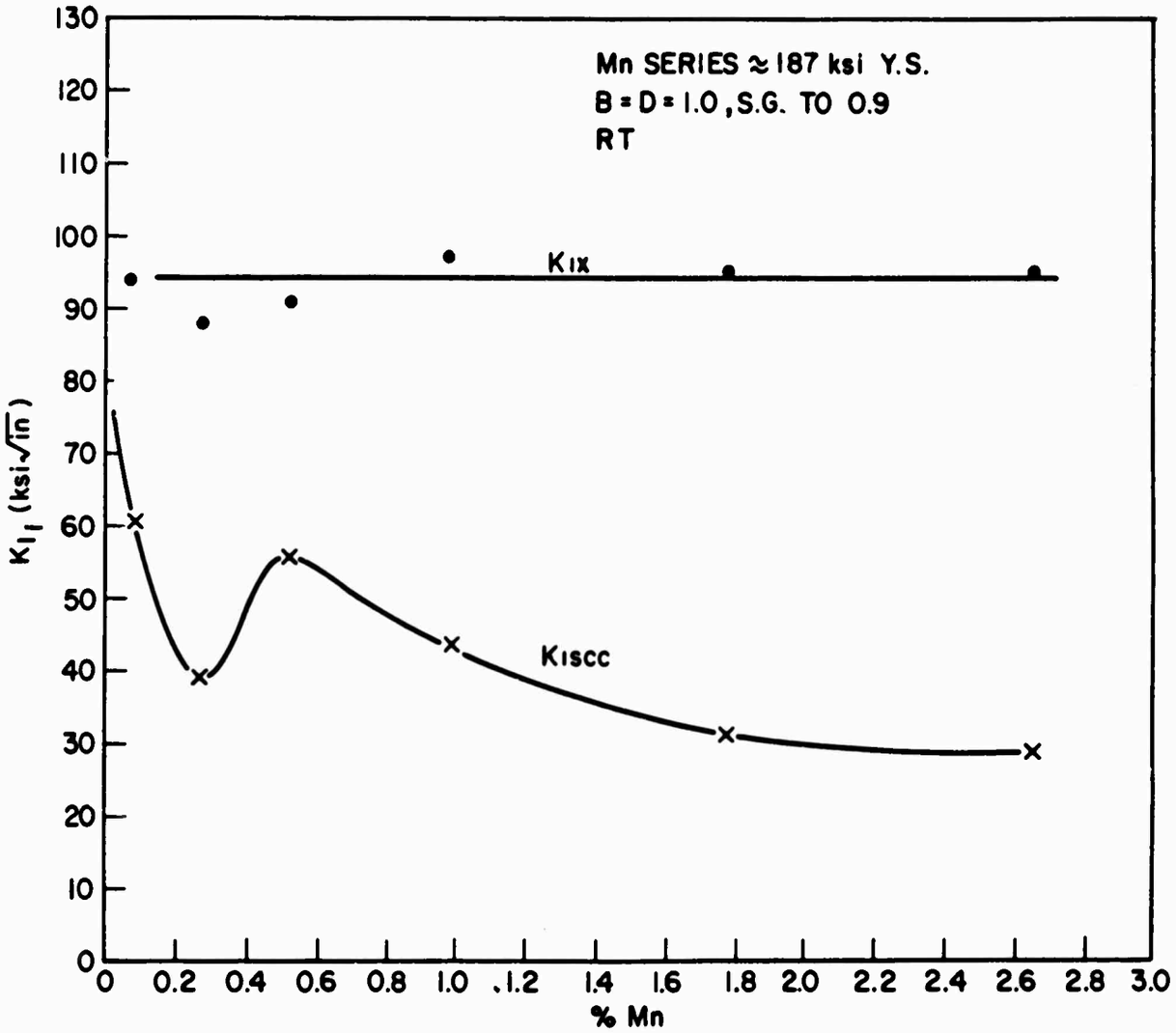

Fig. B-3 - Effects of Mn on the stress-corrosion-cracking resistance of steel similar to AISI 4340 in base composition and quenched and tempered to 187 ksi yield strength.

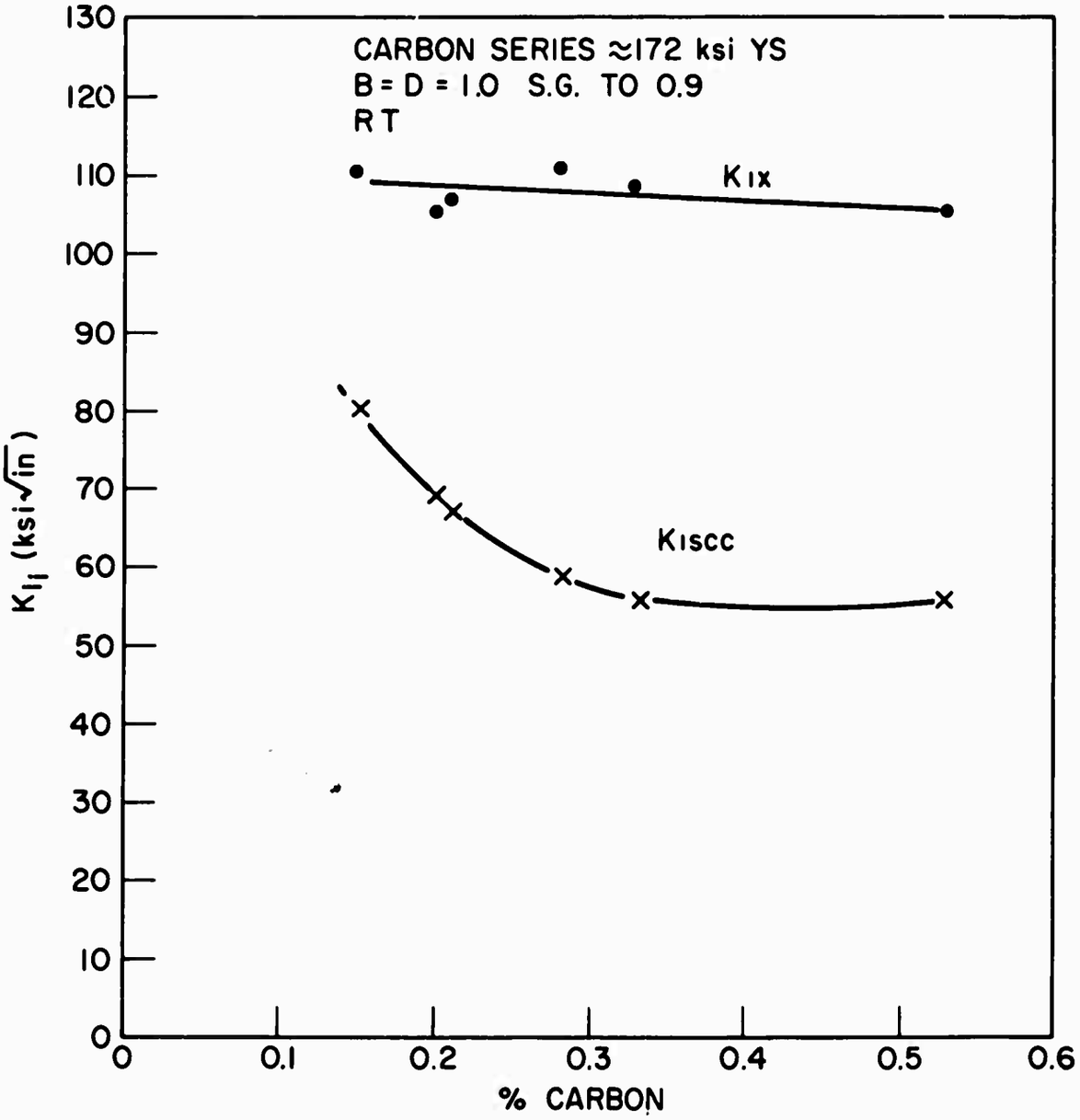

Fig. B-4 - Effects of C on the stress-corrosion-cracking resistance of steel similar to AISI 4340 in base composition and quenched and tempered to 172 ksi yield strength.

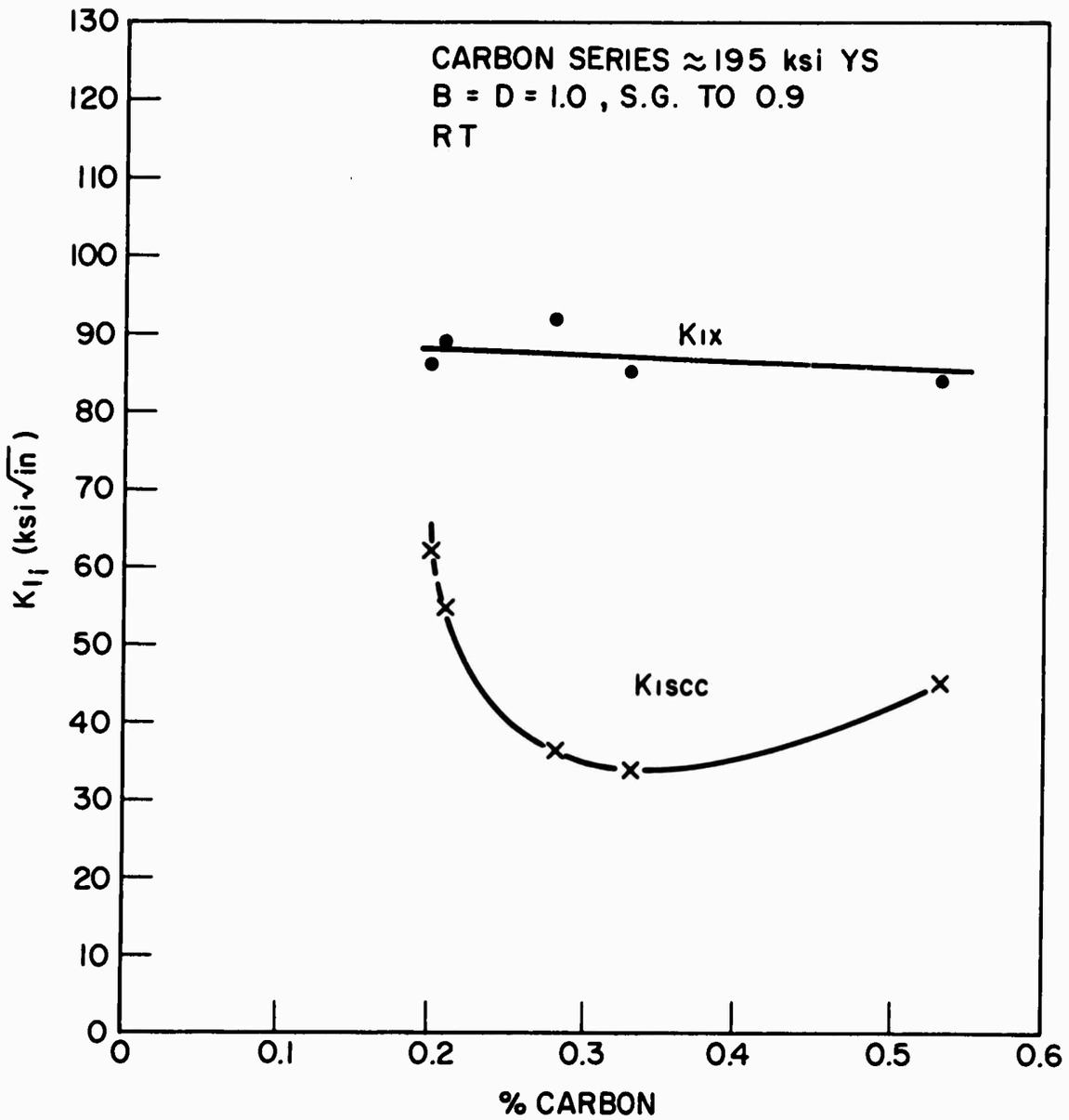

Fig. B-5 - Effects of C on the stress-corrosion-cracking resistance of steel similar to AISI 4340 in base composition and quenched and tempered to 195 ksi yield strength.

made to study the effects of carbon in concentrations up to 0.90 percent. It is hoped to use this series to determine the cause of the rise, if possible, but at least to determine the scope of the phenomenon.

Other alloy series for studying the effects of S in the range 0.004 to 0.24 percent and P in the range 0.002 to 0.27 percent have been made, and specimens are being prepared. A series of steels to be used for a more detailed study of the effects of Cr and Mo (in a lower percentage range than that studied previously) have also been made. A series for studying the effects of Co is planned.

SIMPLIFIED RESEARCH ALLOY

Characterization and Test Techniques

A small, rugged probe consisting of a pH-dependent 1/16-in. solid, cast antimony-antimonous oxide (Sb/Sb_2O_3) electrode in conjunction with a solid 1/16-in. Ag/AgCl reference electrode is currently being utilized at the Naval Research Laboratory to monitor the corrodent pH and metal potential at the advancing edge of a stress-corrosion crack. The electrode reaction and Nernst equation covering this electrode system are as follows:

$$2Sb(s) + 3H_2O \rightleftarrows Sb_2O_3(s) + 6H^+ + 6e^-$$

$$E = E^\circ_{Sb/Sb_2O_3, H^+} - \frac{RT}{F} \ln a_{H^+}$$

The probe can be used in NaCl solutions without a salt bridge and circumvents the two possible errors encountered in the previously described method of Brown, Fujii, and Dahlberg (1), namely: 1) physical staining of the indicator paper by colored soluble corrosion products, and 2) shifting of the color producing equilibria by heavy metal ions or oxidation-reduction reactions.

The probe is pressed against the specimen ahead of the advancing crack tip but is insulated from the specimen by a small, circular shield of open-weave highly

1. B. F. Brown, C. T. Fujii, and E. P. Dahlberg, "Methods for Studying the Solution Chemistry Within Stress-Corrosion Cracks," J. Electrochem. Soc. 116:2 (Feb., 1969) 218-219.

absorbent lens tissue. As the crack advances, liquid within the crack is drawn out by capillary action and wets the lens tissue. The corrodent pH and specimen potential is immediately and simultaneously read by the probe.

Fig. B-6 shows normalized calibration curves for the pH probe in solutions containing ferrous iron. Under reducing conditions, the probe is well behaved over the pH range 2 to 6, but under oxidizing conditions, the oxidation of ferrous to ferric iron interferes and limits the useful range to pH 2 to 5.

This is not a serious limitation as dissolved oxygen is reduced to hydroxyl iron during the corrosion reactions, and the access of additional oxygen to the crack front is restricted. In any event, the pH in the crack front is normally within the range in which there is no interference.

This technique shows great promise for making direct measurements of the electrochemical conditions at advancing crack fronts.

Surface Studies

A study of hydrogen adsorption on pure iron is being carried out at Lehigh University. Because fracture exposes new and indeed atomically clean surfaces of great activity, environment-enhanced crack growth may be controlled by the adsorbate-adsorbent interaction. This study aims to provide further information on the hydrogen adsorption capacity of pure iron at different temperatures, and complements studies of hydrogen-enhanced crack growth in high-strength steels at Lehigh.

A 0.006-inch-diameter, high-purity iron filament, (better than 99.995% purity), is used in this study. The filament was polished chemically and then sealed into an ultrahigh-vacuum system capable of pressures better than 3×10^{-10} torr. The filament was then subjected to the following treatments: (a) degassed for 48 hours, (b) reduced and decar urized in two 16-hour cycles at 600-700°C, (c) argon bombarded for 50 minutes, (d) further decarburized for 16 hours at 700°C, (e) 15

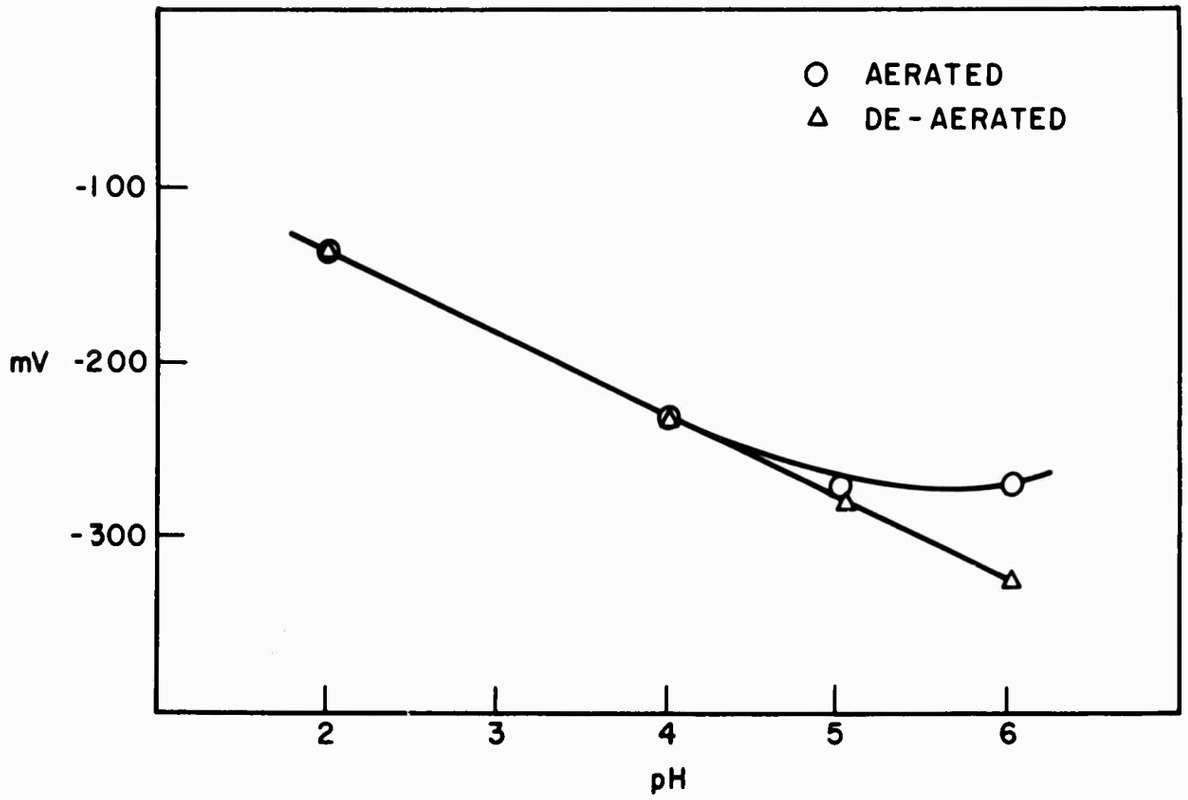

Fig. B-6 - Calibration curves for the Sb/Sb_2O_3 vs Ag/AgCl pH probe (normalized at pH 2) in 0.6M NaCl + 0.01M $Fe(Cl)_2O$ solution.

minutes of heavy argon-bombardment, (150-200 $\mu A/cm^2$ at 550 eV ion energy level), at 5-minute intervals, and (f) final annealing at 850°C. After this treatment, reproducible results could be obtained.

The filament was heated by a regulated dc power supply and its temperature was determined either by pyrometry or by resistance measurements. By adjusting the current, specific temperatures were obtained for the adsorption studies. A sudden flash at 800°C released all of the adsorbed molecules which were recorded either as a pressure increase in a thoriated ionization gauge or as a current increase in the quadrupole gas analyzer. The amount of hydrogen adsorbed as a function of the gas pressure for filament temperatures ranging from 298°K to 630°K is shown on Fig. B-7. The rates of hydrogen adsorption at room temperature will be determined. Further studies of hydrogen adsorption on a 18Ni maraging steel will be made.

A Naval Research Laboratory study for evaluating the effects of chloride ions on the electrochemical behavior of iron in sodium hydroxide solution has been concluded. It was found that corrosion was initiated at chloride ion concentrations of less than one ppm. Current work is involved in further purification of the existing high-purity system. Particular importance is attached to the effect of tungsten since it is the major impurity present in the iron. Over a dozen different effects caused by the presence of small amounts of random impurities have been observed, thus making it possible to assess more accurately the type and the level of impurities in the system at any given time.

To investigate the role of chloride ion in stress-corrosion cracking of materials, water suspensions of αFe_2O_3 were contaminated with various concentrations of Cl^- (added as solid NaCl) and the transient pH effect noted. The potential interference of impurities in studies such as these prompted the use of ultrahigh purity materials in the system under investigation. The reactions between αFe_2O_3 (< 10 ppm total impurities) and CO_2 free, triple-distilled water (30°C) containing various concentrations of NaCl (single crystal) were observed.

Water, contained in a polystyrene apparatus equipped with a magnetic stirrer and glass electrode, was continually purged with oxygen or argon during the course of an experiment. Upon addition of variable amounts (50 to 1000 mg.) of finely

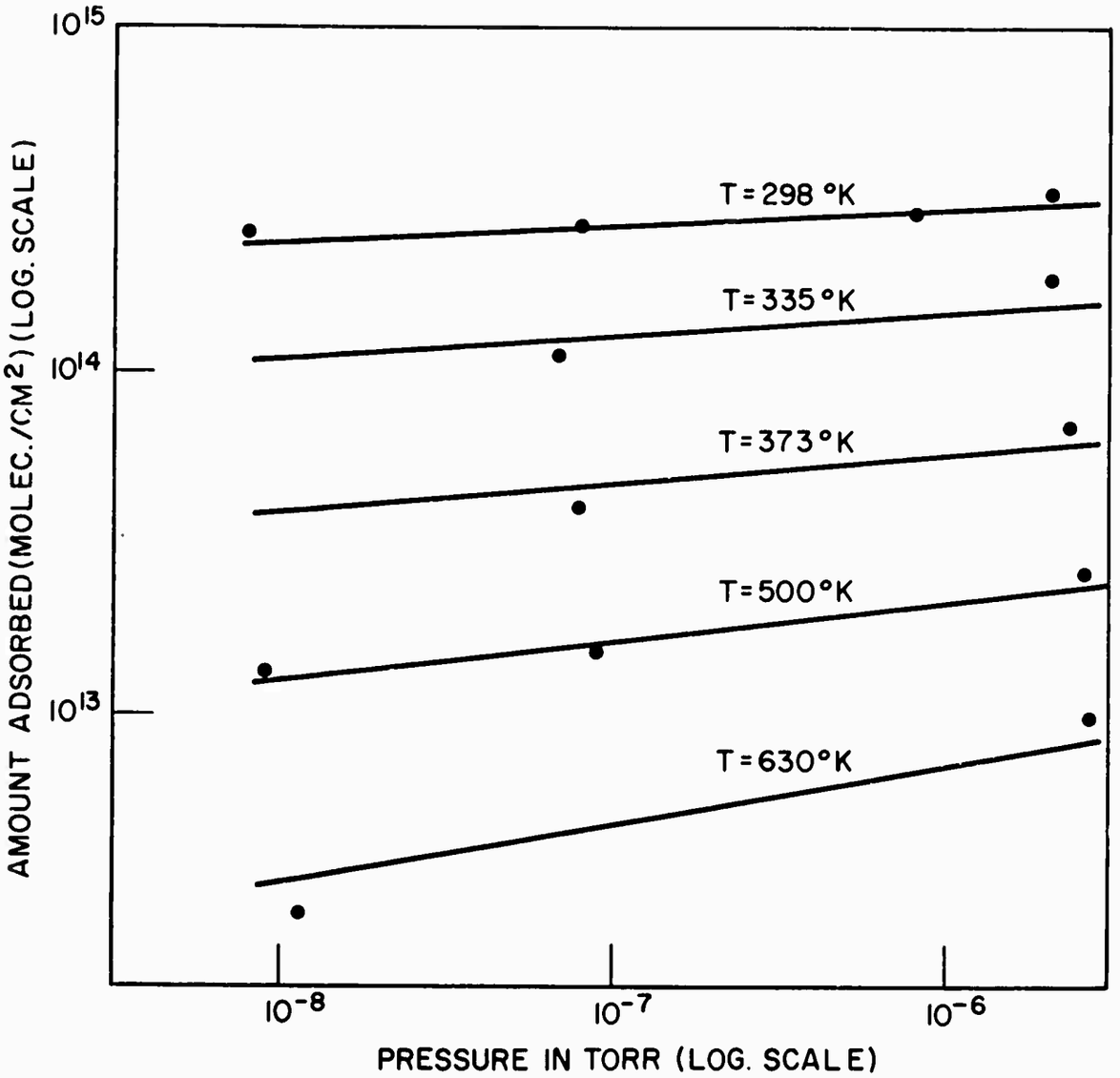

Fig. B-7 - Hydrogen adsorption on high-purity iron as functions of gas pressure and filament temperature.

divided αFe_2O_3 in separate runs, an equilibrium $[H^+]$ increase (10^{-7} to 10^{-4}) was observed in each case. The release or abstraction of H^+ from solution may be explained by the surface hydration of αFe_2O_3 and consequent dissociation of the amphoteric OH groups formed, depending on the environment.

Hydration step:

$$Fe_2O_3 + H_2O \rightarrow 2FeOOH, \text{ or possibly}$$

$$Fe_2O_3 + 3H_2O \rightarrow 2Fe(OH)_3$$

Dissociation as an acid:

$$FeOOH \rightleftarrows FeO_2^- + H^+, \text{ or}$$

$$Fe(OH)_3 \rightleftarrows Fe(OH)_2O^- + H^+, \text{ etc.}$$

Dissociation as a base:

$$FeOOH \rightleftarrows FeO^+ + OH^-, \text{ or}$$

$$Fe(OH)_3 \rightleftarrows Fe(OH)_2^+ + OH^-, \text{ etc.}$$

Similar type experiments on equilibrated αFe_2O_3-H_2O systems are currently in progress, differing in that small amounts of solid NaCl are periodically added to the suspension as new equilibrium conditions are being established. Under these circumstances the $[H^+]$ is observed to be decreasing with increasing concentration of NaCl. As both Cl^- and OH^- are considered to be Lewis type bases, one might expect competition between these anions for active sites on the surface of hydrated αFe_2O_3, reflecting the increase in $[OH^-]$ in solution observed. Further evaluation of results must await both the completion of this particular series and of the radiochemical Cl^- adsorption experiments concurrently in progress.

According to a current theory of stress-corrosion cracking, embrittlement of some stainless steels is caused by hydrogen in a mobile form. Proof of the existence of iron hydrides through the preparation of the pure compounds is of importance in that it would both provide materials for studies of iron-hydrogen bonds and lend credence to the above-mentioned theory of SCC. While preparations of

the iron, cobalt, and nickel hydrides by the Grignard reaction were reported by Ray and Sahai in 1943-46, the present efforts to duplicate these results at the Naval Research Laboratory resulted in easily decomposed etherate iron complexes of low hydrogen content.

Three alternate methods of preparation have since been devised: 1) the reaction between triethyl aluminum and purified $FeCl_3$ in the presence of hydrogen, 2) electrolysis of NH_4Cl in liquid ammonia using iron electrodes, and 3) the sputtering of iron via argon-hydrogen bombardment. Primary effort to date has been directed to the first method.

The reaction of $Al(Et)_3$ with $FeCl_3$ (and H_2) as well as the handling of the product were carried out in argon-filled glove boxes because of the extremely pyrophoric nature of the aluminum alkyl. Using excess alkyl and long reaction times a small amount of black crystalline product was obtained. This product gave X-ray powder lines that is readily indexed as BCC, with a unit cell edge of 3.30Å. This material vigorously evolves gas in a slightly acid solution and contains primarily Fe, Al (10-20%), and H, (as shown by emission and mass spectrographic analyses, with most of the hydrogen evolving in vacuum at a sample temperature of 110-125°C). In contrast to the etherate product from the Grignard reaction, the IR spectrum (KBr pellet) of the alkyl product showed no absorption lines characteristic of organic radicals, although minor amounts of some C_2H_6 related fragments were detected in the gas mass spectrographic results (along with some C_6H_{12} and C_6H_{14} fragments of the solvents). These results are consistent with an iron (aluminum) hydride where the hydrogen has the negative charge associated with a large anionic volume. The existence of well known aluminum hydrides suggests that the product may be stabilized by the presence of aluminum.

C. ALUMINUM ALLOYS

C1. Commercial Alloys

To identify the origin of fracture in high strength aluminum alloys, one must distinguish between fatigue, stress-corrosion cracking (SCC), and monotonic fast fracture. The SCC path in high strength aluminum alloys is intergranular. However, the more brittle of these alloys also show intergranular separation during fast fracture, in the absence of SCC. SCC fracture surfaces which have not been subsequently corroded have rather smooth patches with craze-marks, the so-called "mudcake" or "mudcrack" pattern. This pattern of crazing on a rather smooth surface resembles the cracking of a brittle lacquer layer, rather than secondary cracks in the metal itself, and cannot be detected on monotonic fast fracture surfaces which have been exposed to 3 1/2 percent NaCl for about as long as a stress-corrosion crack of measurable length would take to form. Nor can this pattern be detected on SCC fracture surfaces immersed in salt water after the partially cracked specimen was broken open. Experiments are being conducted to confirm that this mudcrack feature occurs in a brittle tarnish layer formed only during SCC, and to identify the layer.

The corrodent pH has been shown to exert a critical influence on SCC of 7075-T aluminum U-bend specimens in 3.5 percent NaCl solution containing 1 percent K_2CrO_4 (or dichromate). Cracking occurs within 24 hours at pH = 3 but not within six months if the solution is buffered with $KHSO_4/K_2SO_4$ to pH = 4.

(The Naval Research Laboratory)

With regard to the chemistry of stress-corrosion cracking, the critical problem lies in defining the role that anions play in the process. The solution of this problem, of course, must precede any elucidation of the mechanism of stress-corrosion cracking and will form the basis of control methods and the composition of solutions for accelerated test methods.

It is recognized that the manner in which anions enter into the crack initiation process might be different from the manner in which anions participate in crack propagation. The former must be similar to the reactions involved in pitting corrosion and in crevice corrosion, while the latter involves reactions with essentially "oxide-free" aluminum surfaces.

It is proposed that the anion forms surface complexes with aluminum in the following fashion:

$$Al^{3+} + Cl^{-} = AlCl^{++} \quad \text{(surface)}$$

$$AlCl^{++} + xH_2O = Al(H_2O)_x\,Cl^{++} \quad \text{(surface)}$$

$$Al(H_2O)_xCl^{++}\ \text{(surface)} = Al(H_2O)_x\,Cl^{++}\ \text{(solution)}$$

$$Al(H_2O)_xCl^{++} = Al(H_2O)_{x-1}(OH^{-})^{++} + H^{+} + Cl^{-}\ \text{(solution)}$$

The first step must be very rapid, and the hydrated aluminum ion produced in the fourth step is probably the stable species in solution.

This mechanism predicts that the anion is involved in the first ionization step of aluminum. Thus, if the experimental measurement is sufficiently rapid, it will observe a reaction occurring at the very

active aluminum potential. All anions should have an effect based on their relative tendencies to form stable or unstable species. Where the species is very stable it should be observed on the surface (e.g. chromate) or should persist in the solution (e.g. fluoride complexes). When the surface is covered with oxide the anion must penetrate in some fashion to the metal interface (double layer). Thus, pitting will be a time and concentration dependent phenomena.

The experiments described below are intended to test these concepts.

Immersion Experiments

The corrosion rates of high purity aluminum (alloy 1199-H 14) were measured in one-normal halide solutions for times up to 12 weeks. These results are shown in Fig. C-1. The data reported by Pryor (1) are also shown and there is general agreement between the two investigations. The high corrosion rate in fluoride solutions is explained on the basis of the stability, in solution, of complexes ranging from AlF^{++} to $AlF_6^{=}$ as reported by Yatsimirskii and Vasil'ev (2). The greater corrosion rate in iodide solutions is related to the production of free iodine. It is obvious that there is no distinct "chloride effect" in these experiments.

The dissolution rate is a function of the concentration of the halide and the composition of the alloy. Fig. C-2 reports some data on Alloy 7075 in three concentrations of the four halides. The "normal" behavior--a falling off of corrosion with halide concentration is seen in the

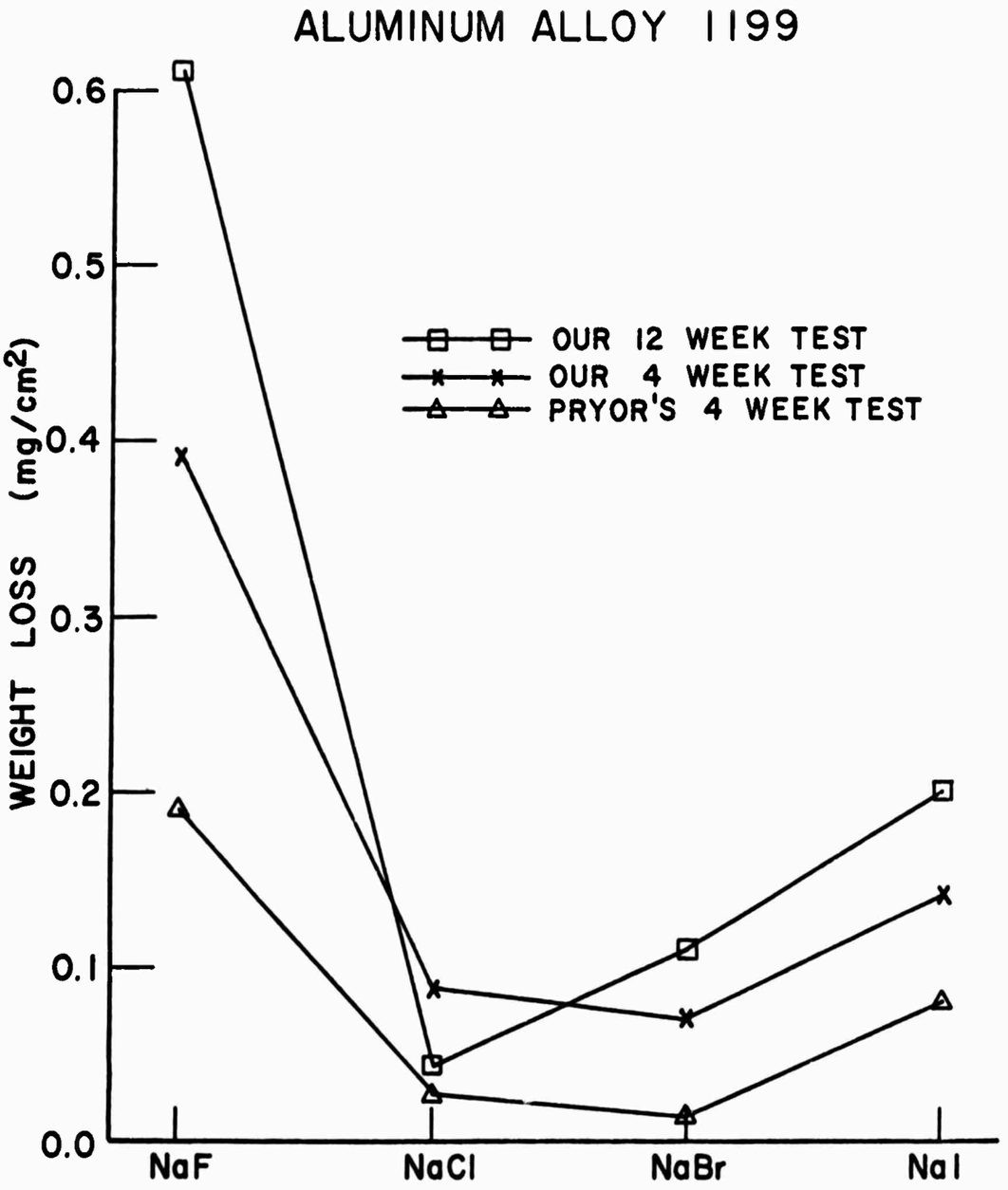

Fig. C-1 - Weight losses of aluminum alloy 1199 in 1.0 N solutions of sodium salts.

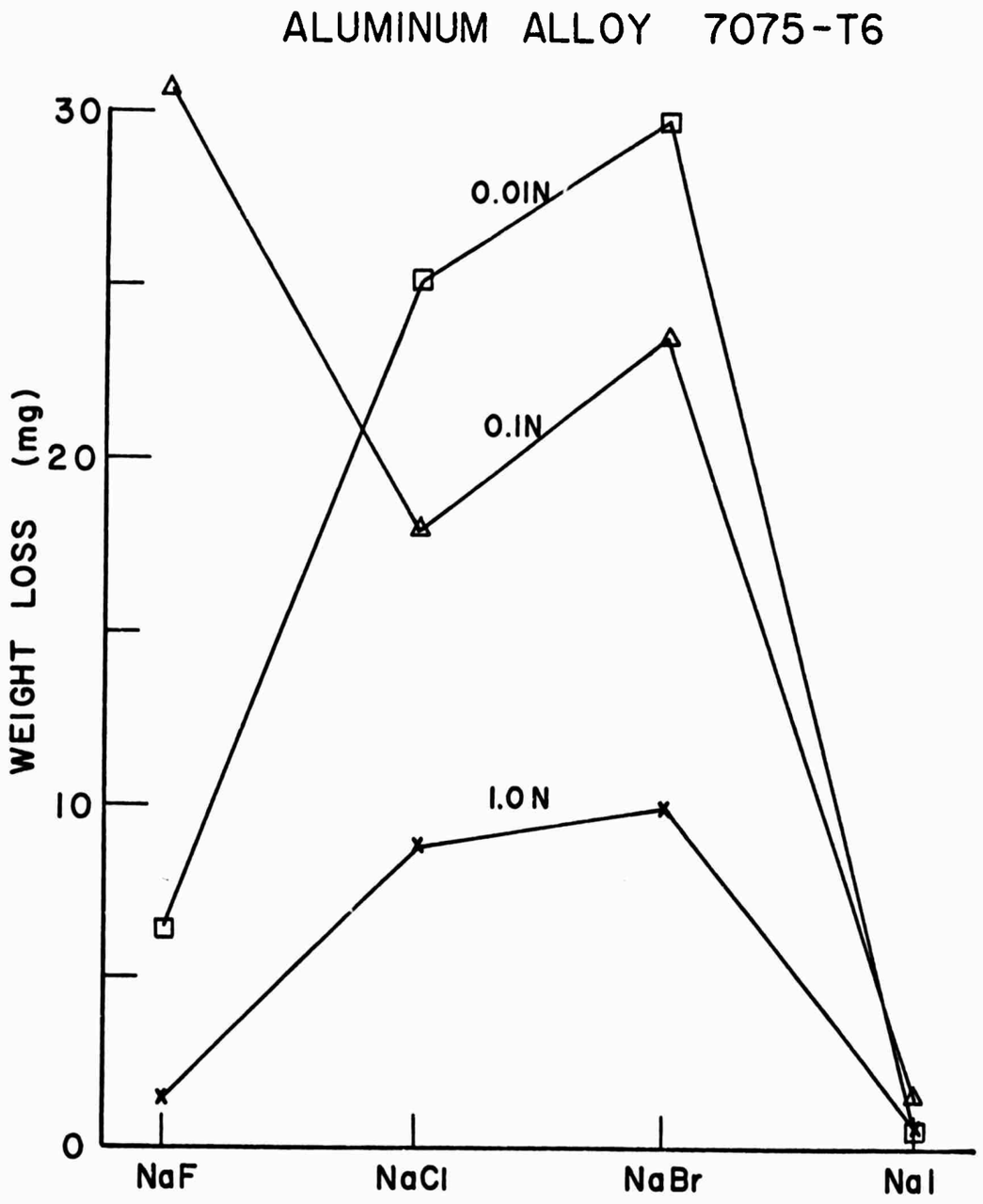

Fig. C-2 - Weight losses of aluminum alloy 7075 in sodium halide solutions.

chloride and bromide solutions. In fluoride solutions there is a maximum rate at 0.1 N and in iodide solutions there is an inhibition effect. Alloy 2024 behaves in a very similar fashion. Of course, any surface complexing must be related to species formed with alloying elements such as Zn, Mg, and Cu as well as aluminum.

Electrochemical Studies

The kinetics of the pitting of aluminum has been investigated by a method similar to that used by Engell (3) and Hoar (4). In this method the electrode is held at some specific potential, either in the passive state or active state, as indicated by the Pourbaix diagram for aluminum, and a sharp rise in current is observed at some "induction" time, τ. In the case of iron the induction time is a function of concentration and is explained in terms of the formation and hydrolysis of ferrous chloride.

The temperature dependence of the induction time has been measured over the range from 15°C. to 40°C. at a solution pH of 6.0 in oxygen saturated solutions. The apparent energy of activation for aluminum alloy 1199 in phosphate buffer is about 30 k cal/mole (Fig. C-3). This value would only have quantitative significance if a single rate-determining step controls over this temperature range, but the high value does suggest a chemical bonding process rather than a weak physical adsorption step.

The concentration-induction time plots have shown a large amount of scatter, and it is felt that at this time the precision of the experiments

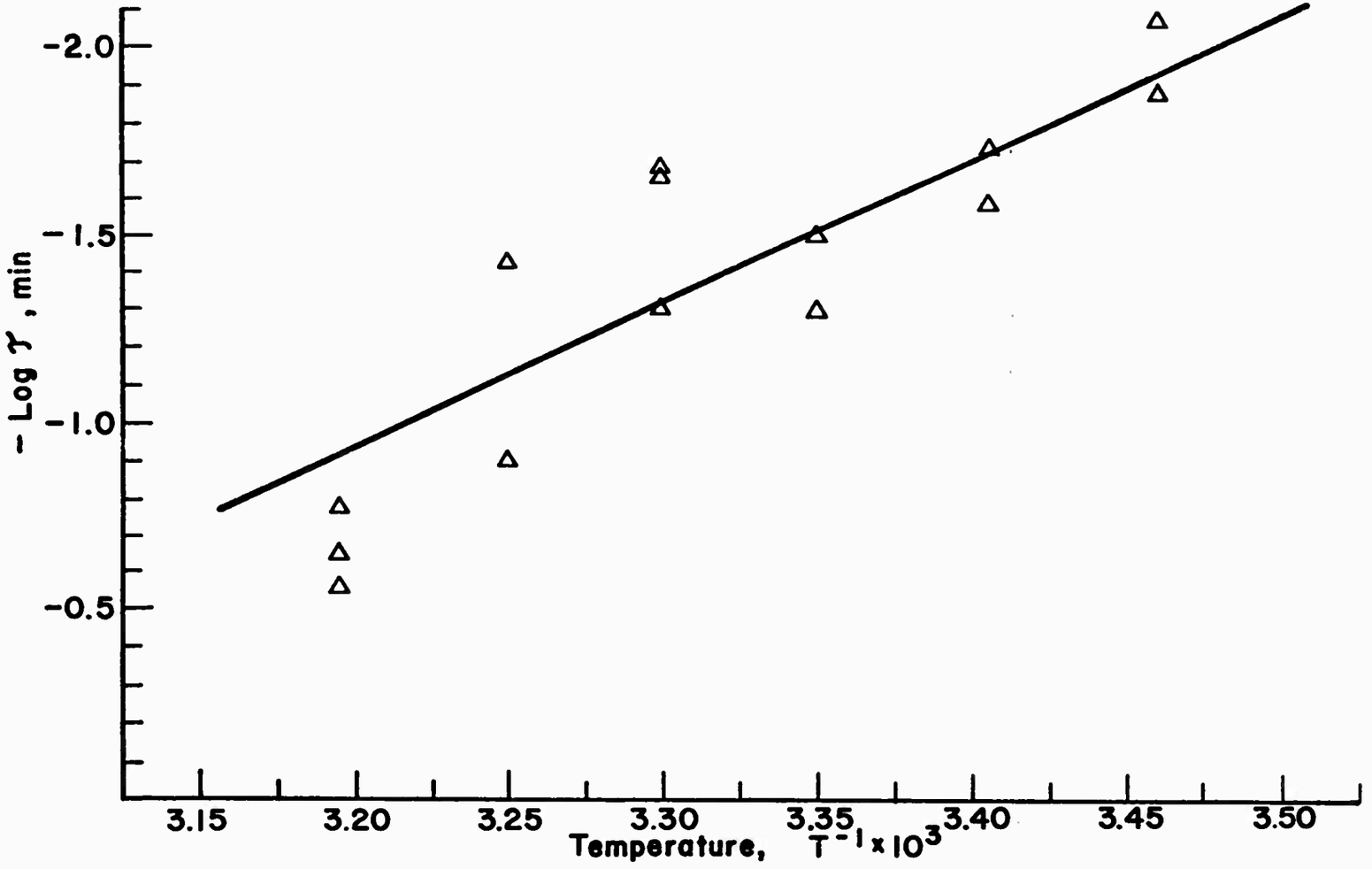

Fig. C-3 - Arrhenius plot. Temperature dependence of induction time for aluminum alloy 1199 from 15° C to 40° C, in phosphate buffer.

is unsatisfactory (Fig. C-4). There is a rough indication that there may be a critical concentration for aluminum pitting similar to that observed with iron (3).

Optical Experiments

Spectrophotometric methods (5, 6) have been used to investigate the presence of complexes such as those predicted in the discussion of the mechanism above. The presence and stability of aluminum-chloro or aluminum-water complexes will indicate the relative rates of step three and step four in the mechanism.

The spectra of aluminum chloride and aluminum nitrate solutions in the UV and visible regions were measured and no evidence for aluminum-chloro complexes were observed. Such species have been observed in non-aqueous solvents such as acetonitrile, benzonitrile, gamma-butyrolactone and ethylene carbonate (7, 8).

A recent NMR study has described the formation of aluminum-anion complexes in various solvents including water (7). In the acidic solution only the signal for the $Al(H_2O)_6^{+++}$ species was observed and in basic solution only the signal for $Al(OH)_4^-$. No evidence was produced for the existence of aluminum-chloro complexes in aluminum chloride solutions.

These studies suggested that the stable species in solution, that is, away from the dissolving aluminum surface is the hydrated aluminum ion. Thus, the aluminum chloro complex, if it does exist, appears in

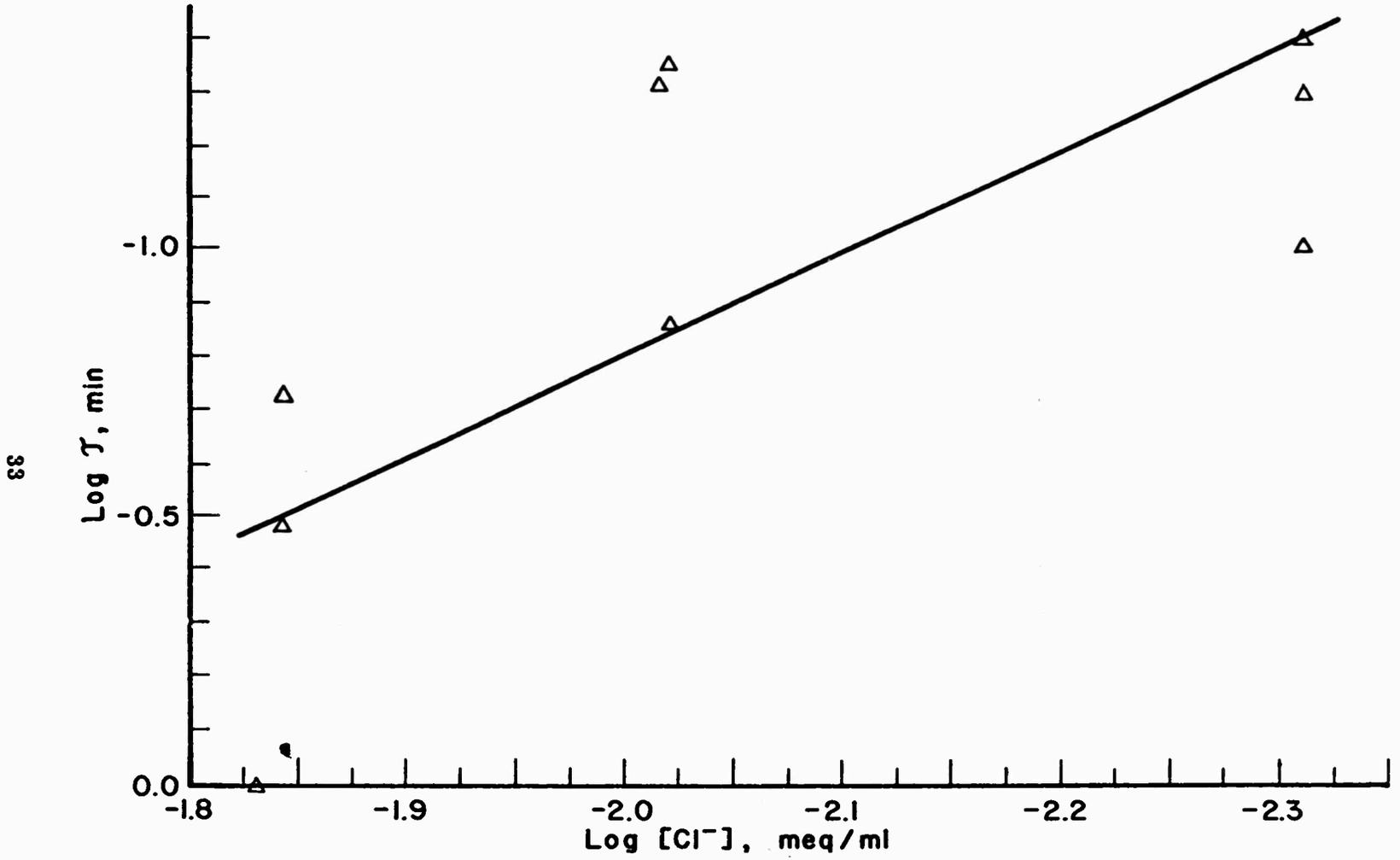

Fig. C-4 - Induction time versus concentration of added chloride ion.

a transitory way, in the double layer at the metal surface.

On the basis of these results, complex formation will be studied with pulsing techniques (9, 10, 11) wherein the structure of the double layer can be observed in short time intervals.

(The American University)

C2. Simplified Research Alloys

The phase transformations, slip lines, mechanical properties and dislocation arrangements in single crystals of an Al, 6%Zn, 2%Mg alloy have been studied with a view to understanding the dislocation-precipitate interactions in these alloys. Thackery (12) has reported that the fully overaged equilibrium η precipitate, $MgZn_2$, can exist in at least six different orientation relationships with the matrix. These are:

Type 1	$(1\bar{2}.0)_\eta$ //$(1\bar{1}1)_{Al}$	$(00.1)_\eta$ //$(110)_{Al}$
Type 2	$(1\bar{2}.0)_\eta$ //$(1\bar{1}1)_{Al}$	$(30.2)_\eta$ //$(110)_{Al}$
Type 3	$(1\bar{2}.0)_\eta$ //$(1\bar{1}1)_{Al}$	$(20.1)_\eta$ //$(121)_{Al}$
Type 4	$(1\bar{2}.0)_\eta$ //$(1\bar{1}1)_{Al}$	$(10.4)_\eta$ //$(110)_{Al}$
Type 5	$(00.1)_\eta$ //$(1\bar{1}1)_{Al}$	$(10.0)_\eta$ //$(110)_{Al}$
Type 6	$(10.0)_\eta$ //$(100)_{Al}$	$(00.1)_\eta$ //$(011)_{Al}$

There is some uncertainty about the sequence of precipitation that occurs in these alloys. From X-ray observations after aging at 200°C, Mondolfo et al. (13) concluded that an intermediate precipitate, with the parameters a = 4.96 Å and c = 8.68 Åwas formed. Thom[illegible] and Nutting (14) observed

spherical particles 30-50 Å in diameter after aging for thirty minutes at 120°C. After a further 30 minutes, small platelets up to 200 Å in length were found. Diffraction of material aged to peak hardness at 120°C indicated that the precipitates were of the intermediate type suggested by Mondolfo et al. They inferred therefore that the precipitation sequence upon aging at low temperatures was:-

$$\text{spherical G. P. zones} \rightarrow \eta' \rightarrow \eta$$

No coherency strains were observed to be associated with η'.

Thackery (12) indicates, however, that an intermediate precipitate with a different structure from that of the equilbrium precipitate is not formed, and that the precipitation sequence is more correctly written:

$$\text{spherical G. P. zones} \rightarrow \eta$$

As pointed out by Mondolfo (15), however, this difference is largely a matter of semantics. The presence of a coherent or partially coherent precipitate which might be designated η' was not discussed by Thackery.

Experimental Details

The alloy used was a high purity Al, 6%Zn, 2%Mg alloy supplied by Aluminum Laboratories, Banbury, Oxon. Single crystals 3.5mm. in diameter and up to 6 inches in length were grown from the melt using a modified Bridgeman technique. Seeding ensured that crystals of only one chosen orientation were prepared. The growth rate normally used was 1cm. an hour. Microprobe analysis of homogenized specimens revealed that a reasonable degree of homogeneity had been achieved

over the center portions of the crystal rods. All specimens were solution treated at 465°C for 2 hours, oil quenched and aged at 135°C. Electropolished tensile specimens with a 1.5 inch guage length were tested at a strain rate of approximately 1×10^{-4} sec^{-1}. All tests were done within one hour of the end of the aging treatment. The shear stress-shear strain curves were calculated assuming single glide up to the symmetry boundary, followed by equal amounts of slip on the primary and conjugate systems.

The {111} planes were spark cut from these specimens and examined in a Phillips 200 electron microscope. All pictures were normally taken in the anomolous transmission region using two beam conditions.

Mechanical Properties

The variation of the resolved yield stress with aging time at 135°C is shown in Fig. C-5. The peak yield strength occurs after approximately 35 hours and the peak yield stress is approximately 10 $kgm.mm^{-2}$. This compares with a peak axial yield stress of 40 $kgm.mm^{-2}$ for the same polycrystalline alloy; this also occurs after approximately 35 hours. The peak ultimate tensile strength actually occurs in slightly overaged specimens.

The shear stress-shear strain curves as a function of aging time are shown in Fig. C-6. The usual change from a low hardening rate to a parabolic stress-strain curve occurs at approximately peak strength. As the yield stress increased with aging time the yield region tends to become more rounded, i.e., the initial hardening rate after yield

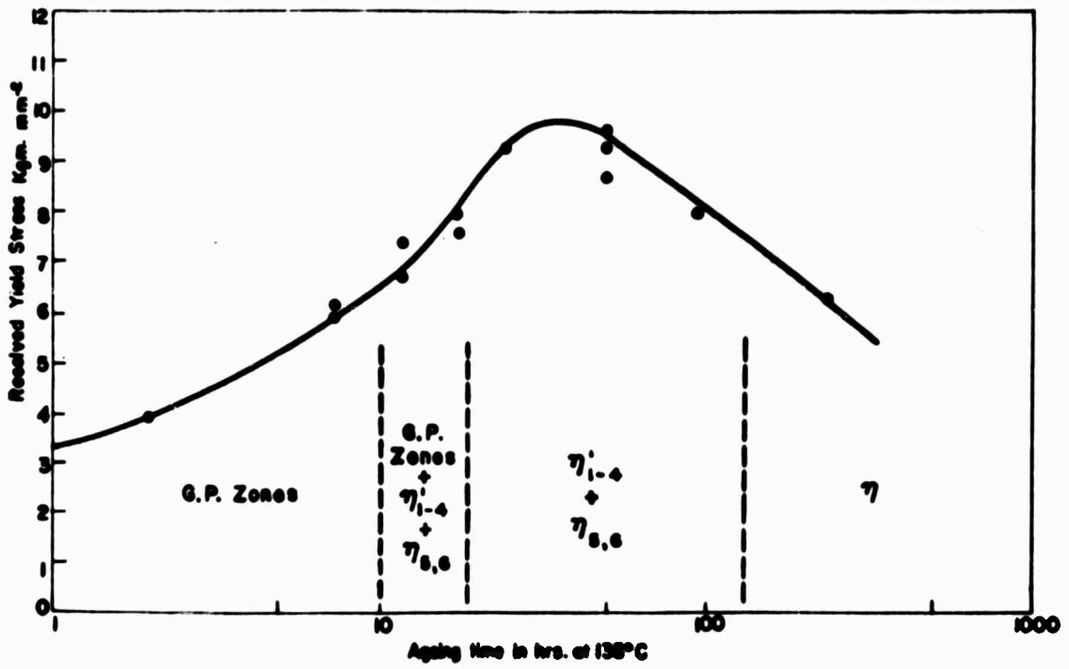

Fig. C-5 - The resolved yield stress at room temperature of Al-6%Zn-2%Mg single crystals as a function of aging time at 135 C.

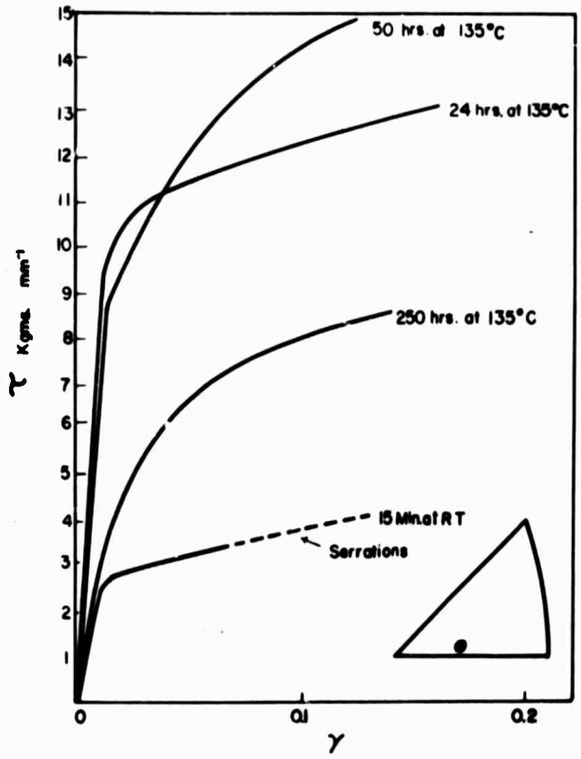

Fig. C-6 - The shear stress-shear strain curves at room temperature of Al-6%Zn-2%Mg single crystals as a function of aging time at 135°C.

increases. The underaged crystals do not show three stages of hardening, and the observed hardening rates are considerably higher than the hardening rate considered typical of stage 1. The hardening rate of as-quenched crystals, for example, was $\approx \mu/300$ compared to a rate of $\approx \mu/3000$ generally recorded for the hardening rate in stage 1 of pure Cu or even pure Al at higher temperatures. As expected, serrations occurred during the plastic flow of as-quenched crystals.

All the crystals tested except those near peak strength were completely ductile in the sense that they necked down to a point. The mode of failure of all underaged crystals that had been aged for at least 10 hours was similar to that outlined by Price and Kelly (16). The main difference between the type of failure in the "as-quenched" and aged crystals was that in the former case necking occurred by the operation of at least two systems, i.e., a chisel point was formed, whereas in the latter case one system predominated. In this instance, therefore, the crystals tended to shear off along the slip plane. For crystals aged close to peak strength, considerable shearing occurred but fracture took place before the specimen necked down completely. As overaging continued, the amount of secondary slip in the necked regions increased although failure still tended to occur by slip on one predominant system.

The slip lines produced after small strains (less than 5% shear) were examined as a function of aging time. There was little change in the slip line morphology on the face parallel to the primary Burgers vector, i.e., the side face. However, at 90° to this face, i.e., the top

face, distinct changes occurred upon aging. Figs. C-7-9 show the appearance of the slip lines on crystals that have been aged at 135°C, for 12 hours, for 50 hours, and for 250 hours. Fig. C-7 shows that the slip lines of the primary system are quite wavy when viewed on the top face. Trace analysis indicates that the secondary bands shown in Fig. C-7 probably belong to the cross slip system. This wavy appearance persists up to a stress level of about 7.5 kgm. mm^{-2}. Upon further aging the slip lines become intense and straight as shown in Fig. C-8. This lamellar appearance is maintained in the overaged crystals, Fig. C-9, although the average step height for a given strain generally decreases with aging. The most intense lamellar slip lines were observed at peak strength.

As Fig. C-8 shows, occasional traces of slip on the critical system were observed. This, however, is a result of the initial orientation which in some cases was close to the symmetry boundary. It should be noted, however, that sharp straight slip lines could be observed on only one system even when the stress-strain curve was parabolic.

The sub-grain size in the heat-treated specimens was normally about 2mm. Electron microscopy indicated that both precipitate free zones and equilibrium precipitates were associated with these subboundaries even after aging for only 10 hours. The lamellar slip lines were observed to pass through the subboundaries with only a slight deviation in direction, e.g., Fig. C-8. The wavy slip lines of Fig. C-7, however, frequently nucleated secondary systems at subboundaries as shown in Fig. C-10.

Fig. C-7 - Slip lines on the top face of a crystal aged at 135°C for 12 hours ($\gamma \approx 0.5$).

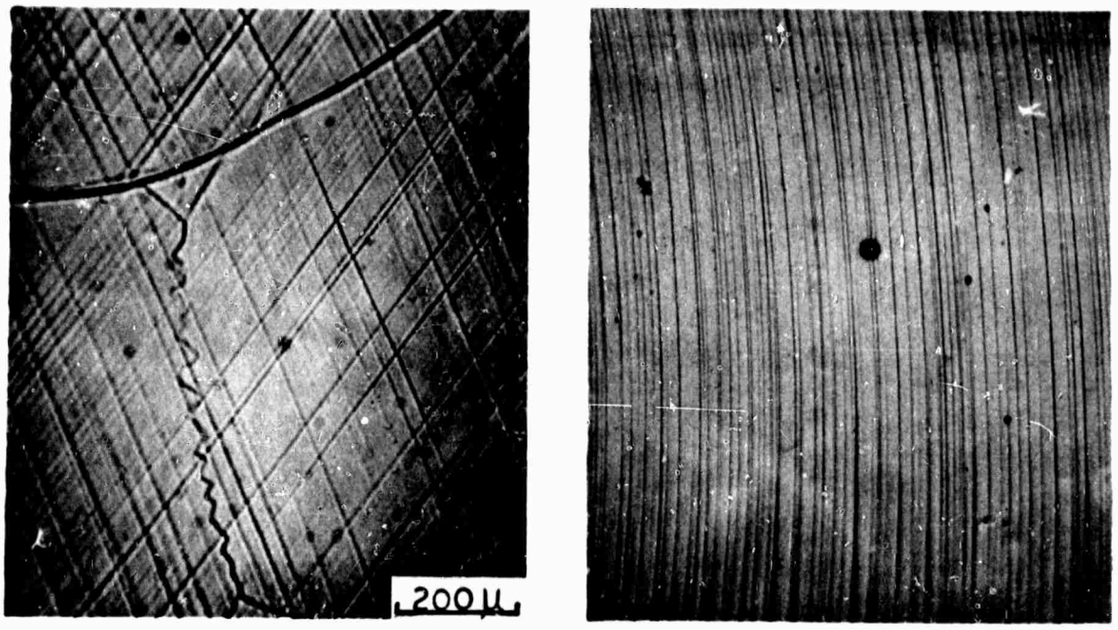

Fig. C-8 - Slip lines on the side (left) and top (right) faces of a crystal aged at 135°C for 50 hours.

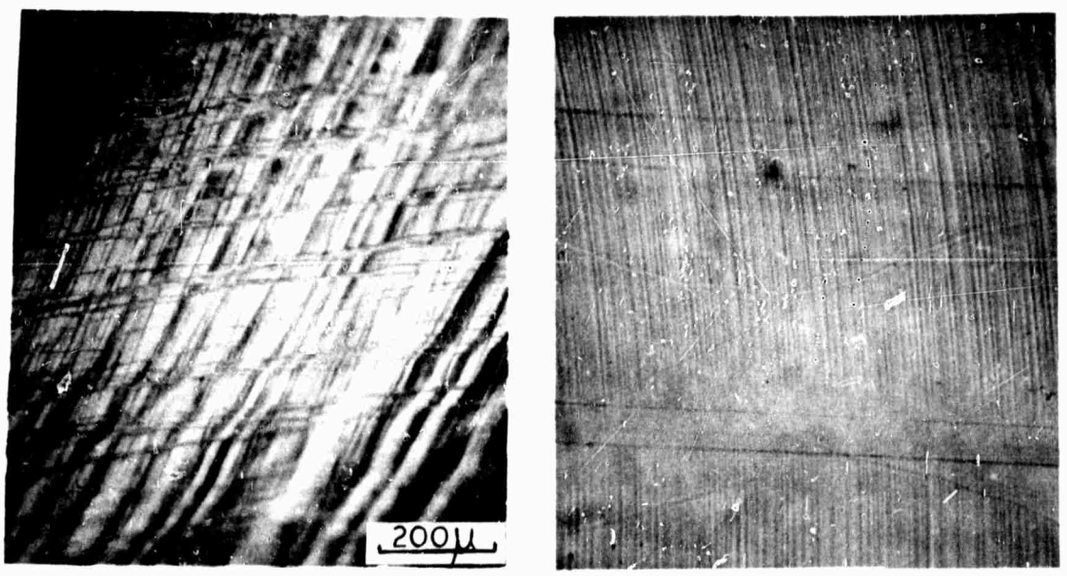

Fig. C-9 - Slip lines on the side (left) and top faces of a crystal aged at 135°C for 250 hours. The side face is taken near the necked part of a crystal. The top face corresponds to a shear strain of approximately 0.05.

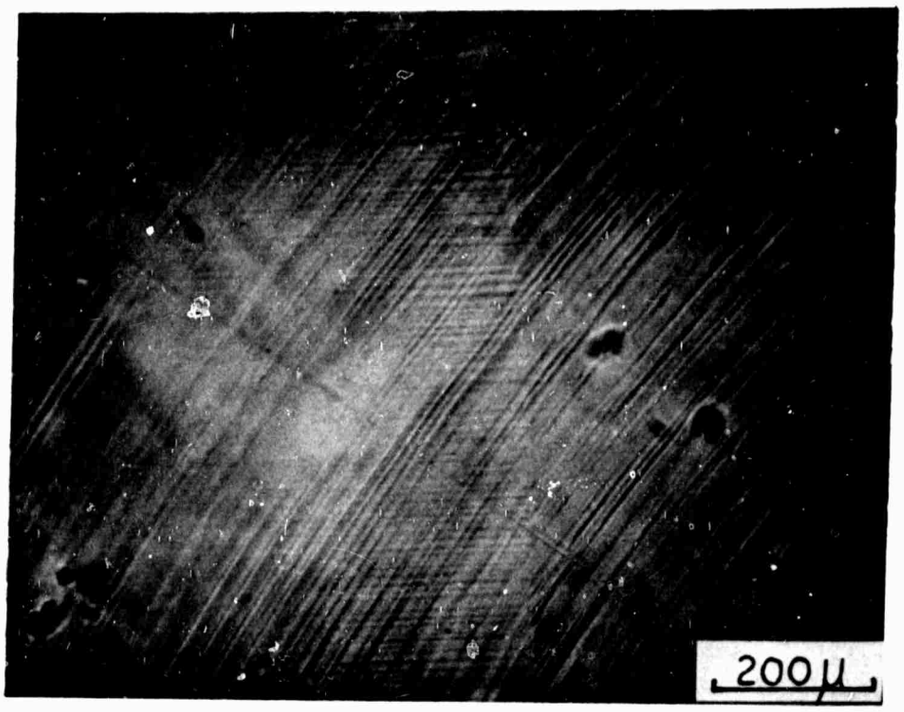

Fig. C-10 - The nucleation of a secondary system at a subboundary in a crystal aged for 12 hours at 135°C.

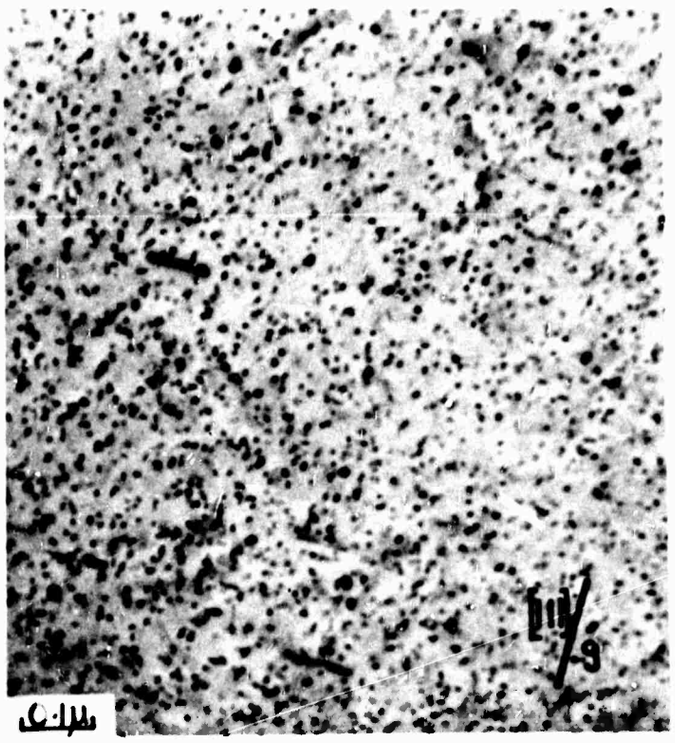

Fig. C-11 - The precipitate morphology observed after aging for 24 hours at 135°C.

Several single crystals were tested for their stress-corrosion resistance after aging for 12, 24 and 50 hours. These tests were done at constant deflection using a circulating 3.5% sodium chloride solution. Although these crystals exhibited pitting corrosion, cracks were not observed to grow even after loading above the yield stress for as long as 200 hours. The slip steps often appeared to be anodic. Similar polycrystalline specimens aged to peak strength and loaded in sodium chloride to eighty percent of the yield stress failed in about 20 minutes.

Precipitate Structure and Morphology

The precipitate morphology observed after aging for 24 hours at 135° C is shown in Fig. C-11. This picture was taken in a thin region of the foil; the approximate thickness was 300Å. While the precipitate spots on a ⟨111⟩ matrix diffraction pattern are very diffuse, comparison with the same pattern from a slightly overaged crystal suggests that the η or η' phase was present. Although a few precipitates were elongated in the ⟨110⟩ directions, the majority appear to be approximately spherical or even disc shaped with a diameter of about 100Å.

Figs. C-12 and 13 show the {111} plane of a specimen aged for 80 hours at 135° C. The precipitate morphology is very complex. Approximately fifty percent of the precipitates seem to be lath shaped while the remainder are not characterized by any well-defined geometry. In Fig. C-12 several large precipitates which lie in the plane of the foil, e.g., at A (this is a type 1 precipitate). show dislocation ring contrast, while pre-precipitates at B in Figs. C-12 and 13 exhibit well-defined strain fields with the line of no contrast perpendicular to $\bar{g}$. This indicates that these precipitates possess a coherent or partially coherent interface.

A. Dislocation ring contrast B. Strain field contrast

Fig. C-12 - The precipitate morphology observed after aging for 80 hours at 135°C.

C. Displacement fringe contrast of type 1 precipitates

Fig. C-13 - The precipitate morphology observed after aging for 80 hours at 135°C.

Electron diffraction of fully overaged precipitates confirmed the relationships given by Thackery while diffraction of only slightly overaged precipitates displaying strain field contrast confirmed relationships 1-4. The maximum length of partially coherent type 1 precipitates appears to be approximately 1800 Å. Observations on fully incoherent type 1 precipitates indicates that the upper limit on the thickness of partially coherent plates is approximately 75 Å. Precipitates of type 2-4 have not been observed to possess strain fields when longer than 750 Å. Precipitates not having a lath shape have not been observed to possess any strain fields. In general precipitates of type 1 are always observed to be longer than precipitates of types 2-4.

Examination of displacement fringes, e. g., at C in Fig. C-13, indicates that the habit plane of type 1 precipitates is $\{111\}_{Al}$. The displacement fringes that have been observed for precipitates of types 2-4, e. g., at D in Fig. C-13 are, however, less intense and usually have a wider spacing than those of type 1. Although the alignment of these fringes is not clearly delineated, it appears that some correspond to a $\{111\}_{Al}$ habit while others are more consistent with a habit near $\{211\}_{Al}$.

Examination of the strain contrast as a function of reflection condition indicates that the maximum value of the displacement vector is perpendicular to the precipitate plate, i. e., in the $\langle 111 \rangle$ direction. There may, however, be smaller components in the plane of the plate.

It was noticed, depending on the dispersion, the size of the precipitates or zones, and the strain, that deformation occasionally produced either

dissolution or growth of the precipitates. The duplex precipitate distribution shown in Fig. C-14 for example was produced upon deformation of a crystal previously aged for 24 hrs. at 135°C. The precipitates produced as a result of deformation generally had very irregular shapes.

Discussion

The present results indicate that the sequence of precipitation in Al,6Zn,2Mg alloys is very complex. For precipitates of types 1-4 there is definite evidence of a partially coherent precipitate with the same structure as the equilibrium η precipitate. The usual description of an intermediate partially coherent precipitate will be adopted, i.e., this precipitate will be designated η'. The sequence of precipitation for types 1-4 appears to be:

$$\alpha \rightarrow \alpha' + \text{G.P. zones} \rightarrow \alpha'' + \eta' \rightarrow \alpha''' + \eta$$

where α represents the solid solution.

No evidence for the independent nucleation of any of these phases has been obtained. Although the T phase has been indicated to be the equilibrium phase at least at 200°C, it has not been observed in this study. The complexity of the precipitate morphology, however, means that this phase or even the X phase suggested by Thackery might easily be overlooked. The changes in lattice parameter between η' and η observed by Mondolfo et al. was attributed to internal atomic rearrangements. It is possible, however, that these changes may occur by the replacement of Al in $Mg_a\ Zn_b\ Al_c$. It has been indicated by Laves and Witte (17) that this phase has the $Mg\ Zn_2$ structure provided the electron-

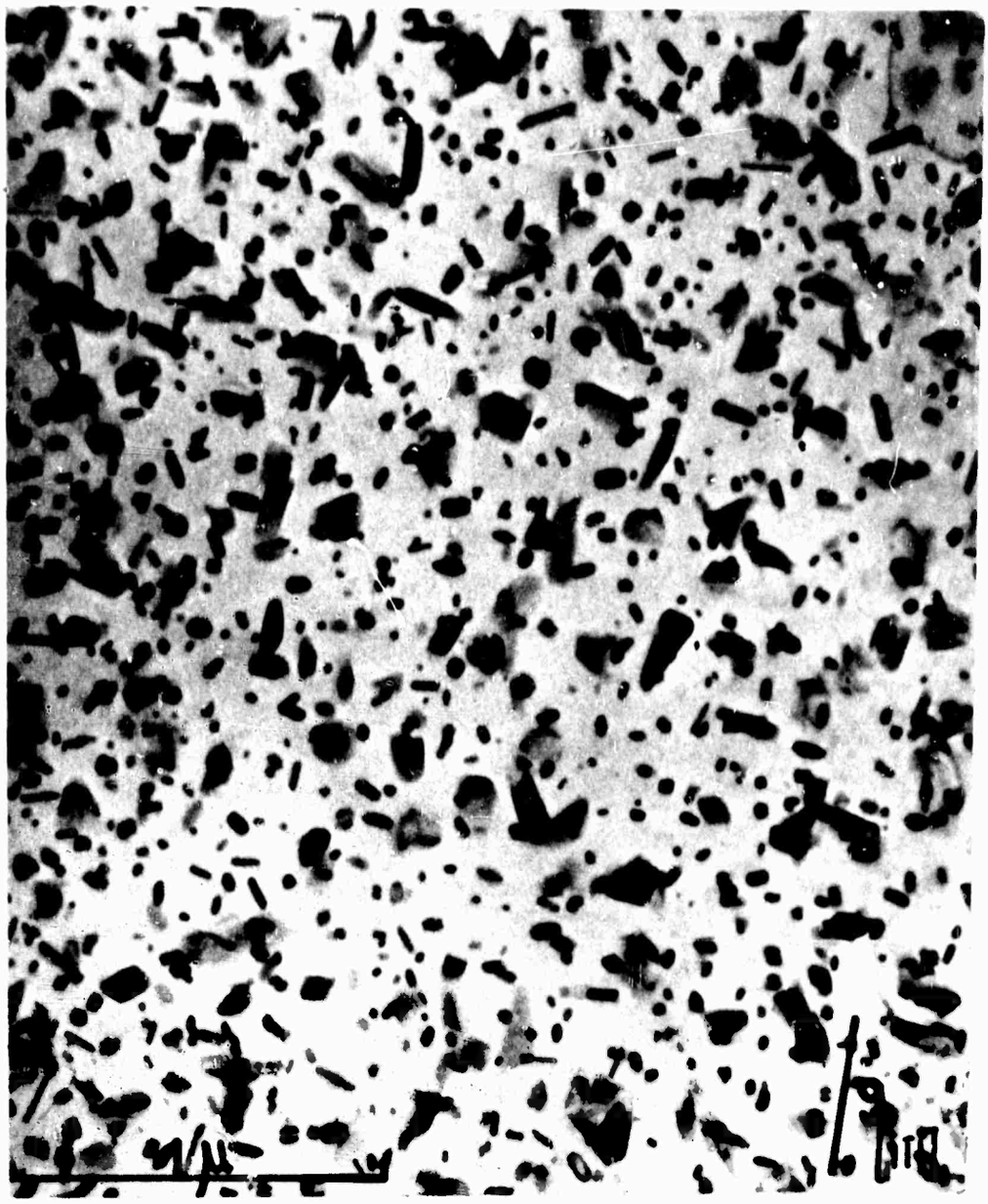

Fig. C-14 - A duplex precipitate distribution produced during gross deformation of a specimen aged for 24 hours at 135 C.

atom ratio is between 2.0 and 2.1.

For precipitates of types 5 and 6 it seems probable that a coherent or partially coherent interface is not formed and that the more correct sequence should be written:

$$\alpha \rightarrow \alpha' + \text{G.P. zones} \rightarrow \alpha'' + \eta$$

The approximate regions over which these changes occur are shown in Fig. C-5. As aging proceeds, the lattice parameters of η may change towards their equilibrium value as indicated by Mondolfo et al. although this has not been verified in this study. The lack of marked diffraction effects in the region marked G. P. zones may hide the presence of other stages. The zones for example may become ordered. If one examines the structure of the η phase, it is apparent that coherency between the matrix and precipitate is difficult to achieve across any interface. Coherency cannot, for example, be achieved between the (0001) plane of the η precipitate and the {111} matrix planes as has occasionally been suggested. Similarly, coherency does not exist between the $\{12.0\}_{\eta}$ and $\{111\}_{Al}$ planes. Strain fields, characteristic of a displacement vector in the {111} direction perpendicular to the plate, have been shown, however. It seems likely, therefore, that the {111} and {1120} planes are constrained such that matching occurs around the rim of the plate. This does not take place across any well-defined plane, however, as strain fields have been observed around the whole rim of the precipitate. Using the values of a = 4.96 and c = 8.68 given by Mondolfo et al.(13) for the lattice parameters of η' then, $d_{(11\bar{2}0)_{\eta'}} = 2.465$ Å and $d_{(111)_{Al}} = 2.337$ Å, i.e., there is only a 5.5% difference between the d spacings.

It is instructive to discuss why so many orientation relationships between the precipitate and matrix exist in this alloy. The G. P. zones are usually described as spherical although the present observations suggest they have irregular shapes which may approximate to a sphere. Some zones definitely appear to be disc shaped. The criteria normally considered to control precipitate morphology are the presence of low energy or coherent interfaces and the strain energy produced by differences in volume of the precipitate and matrix containing equal numbers of atoms. The volume change and coherency strains may also produce local tensile or compressive stresses in the matrix which would influence diffusion in the vicinity of the interface. External stresses may also have this effect. Precipitates of type 1, which are observed to grow most rapidly in the $\langle 110 \rangle$ matrix directions, i.e., in the (0001) precipitate direction, predominate due to the small volume change and the low surface energy around the rim of the plate. These considerations also apply to precipitates of types 2-4 although the volume changes are larger. These precipitates, therefore, do not occur as frequently, nor do they grow as fast as those of type 1. Type 5 precipitates may also possess a low energy interface around their rim if the $\{111\}$ matrix planes are constrained to match alternate (0001) planes of the precipitate. No strain fields have been observed around these precipitates, however. Precipitates of type 6 are favored by a small volume change. In general it seems that the large number of precipitate matrix orientation relationships and the presence of irregular shaped precipitates is due to the lack of any pronounced low energy coherent interfaces.

Mechanical Properties

The change from a low to a high work-hardening rate as aging continues is usually attributed to the production of geometrically necessary dislocations. These dislocations are required to accommodate the strain around a particle that has not been sheared. A high hardening rate is also usually accompanied by very diffuse slip lines, e. g., the Al-Cu or Fe-Mo systems. In this case, however, very sharp slip lines occur on only one slip system even when the hardening rate is high. Using the Orowan criterion it would seem that even in considerably overaged crystals that the precipitate spacing is too small to correspond to the applied stress. It is concluded therefore that the precipitates must be cut and that the high hardening rate is due to the production of interface dislocations as the precipitate is sheared. It is noted that for all six precipitate-matrix orientation relationships, the most probable slip planes and slip vectors in the matrix and precipitate are not parallel. The observation that the slip lines on slightly overaged crystals have a lamellar appearance suggests that very little cross slip is occurring. This also indicates that the precipitates are being cut. It seems that the dislocations do not begin to bow between the precipitates until considerable softening has occurred.

The manner in which the aged crystals fail, i. e., by shear on one slip plane seems to depend on the difficulty of large scale slip occurring on secondary systems. For a crystal aged to peak strength it has been observed that the dislocation density in the slip bands is

very high. This high density in the primary system causes considerable latent hardening on the secondary systems. Deformation therefore continues to occur on the primary system.

Comparison with Polycrystals

It is generally observed that polycrystals of Al-6Zn-2Mg alloys aged to peak strength exhibit very little ductility and stress corrode very rapidly. Single crystals, however, exhibit considerable ductility and stress corrode very slowly if at all. Tests on bamboo structures produced by the strain anneal technique indicated that if the slip bands did not intersect the grain boundaries, then they behaved in a similar way to the single crystals. If, however, the slip band impinged on the grain boundary, as in Fig. C-15, then the grain boundary would break open. It would seem that the stress concentration at the head of slip band causes the relatively weak grain boundaries to fail rather than causing secondary systems to nucleate in the adjacent grain. The resistance to grain boundary fracture, therefore, seems to depend on the relative magnitudes of the matrix shear stress, τ_m, the grain boundary fracture stress, $\sigma_{G.B.}$, and the relative rates of increase with time(t) of the tensile stress on the boundary $\sigma_T(t)$ and the shear stress in the adjacent grain on the most highly stressed system $\tau_r(t)$. The increase of σ_T and τ_r will then depend on the geometry, dislocation dynamics and stress state. Clearly if σ_T becomes greater than $\sigma_{G.B.}$ before τ_r is greater than τ_m, then grain boundary failure will occur.

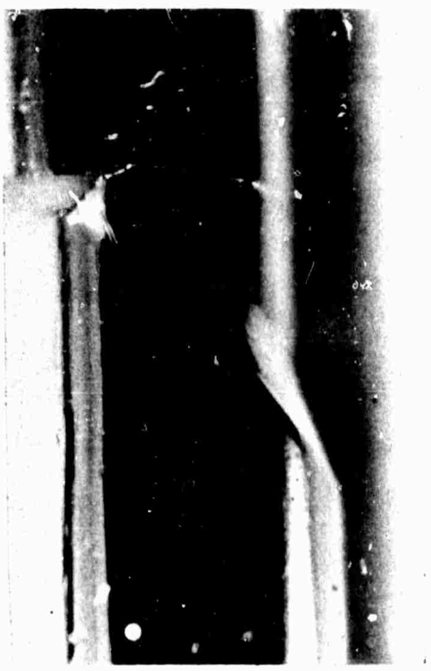

Fig. C-15 - Fracture of a grain boundary by slip in a bamboo crystal aged 12 hours at 135 C. (10X magnification)

Similar considerations can be discussed with reference to stress-corrosion cracking. It seems that the presence of a low angle boundary, its associated grain boundary precipitates and P.F.Z. is not sufficient in itself to promote stress-corrosion cracking. One can attribute this to the ease with which slip is nucleated in the adjacent sub-grain.

(Carnegie-Mellon University)

References

1. M. J. Pryor, Zeit. für Elektrochemie 62, 782-794 (1958)
2. K. B. Yatsimirskii and V. P. Vasil'ev, "Instability Constants of Complex Compounds" D. Van Nostrand and Co., Inc., Princeton, N. J. (1966)
3. H. J. Engell and N. D. Stolica, Zeit. für physik. Chemie. N. F., 20, 113-120 (1959)
4. T. P. Hoar and W. R. Jacob, Nature, 216, 1299-1301 (1967)
5. L. Newman and D. Hume, J. Am. Chem. Soc. 79, 4571 (1957)
6. T. Williams, J. Inorg. Nucl. Chem. 24, 1215 (1962)
7. H. Haraguchi and S. Fujiwara, J. Phys. Chem. 73, 3467 (1969)
8. F. W. Breivogel and M. Eisenberg, Electrochemica Acta 14, 459 (1969)
9. T. Hagyard and J. R. Williams, Trans. Fara. Soc. 57, 2288 (1961)
10. J. S. Riney, G. M. Schmid, and N. Hackerman, Rev. of Sci. Inst. 32, 588 (1961)
11. M. W. Breiter, Electrochimica Acta, 12, 679 (1967)
12. P. A. Thackery, J. Inst. Met., 96, 228, (1968)
13. L. F. Mondolfo, N. A. Gjostein, and D. W. Levinson, Trans. Am. Inst. Met. Engrs., 206, 1378, (1956)
14. G. Thomas and J. Nutting, J. Inst. Met., 88, 81, (1959-60)
15. L. F. Mondolfo, J. Inst. Met., 97, (1969)
16. R. J. Price and A. Kelly, Acta Met., 12, 979, (1966)
17. F. Laves and H. Witte, Metallwirtschaft, 15, 840, (1936)

D. ABSTRACTS OF ARPA-GENERATED MANUSCRIPTS, REPORTS, AND TALKS

The Boeing Company

1. M. V. Hyatt, "Use of Precracked Specimens in Stress-Corrosion Testing of High-Strength Aluminum Alloys," Boeing Document No. D6-24466, November 1969

> Resistance to stress-corrosion cracking of 10 high-strength aluminum alloys in a variety of heat-treatment conditions has been measured using precracked double cantilever beam (DCB) specimens. A new technique is described, and stress-corrosion crack growth rates for the alloys tested are presented as a function of the plane-strain stress intensity K_I. Crack growth rates for alloys in the T3 and T6 tempers showed both K_I-independent and K_I-dependent behavior, whereas alloys in the more resistant tempers showed only K_I-independent behavior over the K_I range studied. Double cantilever beam specimen data correlated with established trends from smooth specimens tested by alternate immersion in 3.5% NaCl solution. From the crack growth rate data and the speed and simplicity with which it is obtained, it is concluded that the DCB specimen will be highly useful for (1) comparing and rating alloys, (2) developing new alloys and heat treatments, (3) comparing the effects of environments, (4) achieving or ensuring product uniformity, and (5) studying mechanisms of cracking.

2. M. V. Hyatt, "Use of Precracked Specimens in Selecting Heat Treatments for Stress-Corrosion Resistance in High-Strength Aluminum Alloys," Boeing Document No. D6-24467, November 1969

> Three techniques using precracked double cantilever beam (DCB) specimens have been employed to measure resistance to stress-corrosion crack propagation as a function of the degree of overaging in the alloy 7075. Two techniques used single DCB specimens containing aging gradients along their lengths. The third technique used multiple DCB specimens, each one having a different heat treatment. All three techniques gave similar results, but stress-corrosion resistance as a function of heat treatment was determined most rapidly using

separate DCB specimens having different heat treatments. Data from this study suggest that DCB specimens would be useful in several other stress-corrosion study areas, including that of thermo-mechanical treatments for aluminum alloys.

3. M. V. Hyatt, "Effects of Residual Stresses on Stress Corrosion Crack Growth Rates in Aluminum Alloys," Boeing Document No. D6-24469, November 1969

Stress-corrosion crack growth rate data obtained as a function of the plane-strain stress intensity using double cantilever beam specimens of 7079, 7075, and 7175 are presented. The effects of quenched-in residual stresses on crack growth rates in specimens of this design are discussed, and methods of eliminating the residual-stress problem are presented.

4. M. V. Hyatt, "Effects of Specimen Geometry and Grain Structure on Stress-Corrosion Cracking Behavior of Aluminum Alloys," Boeing Document No. D6-24470, November 1969

Effects of side grooves, grain structure, and thickness on the growth behavior of stress-corrosion cracks in double cantilever beam (DCB) specimens of aluminum alloys are discussed briefly. Problems encountered in testing DCB specimens from aluminum die forgings are also discussed.

5. M. V. Hyatt, "Effect of Quenching Rate on Stress-Corrosion Crack Growth Rates in 2024-T4 Aluminum," Boeing Document No. D6-24471, November 1969

Stress-corrosion crack growth rates in double cantilever beam specimens of 2024-T4 aluminum quenched at two rates from the solution-treatment temperature were compared. The specimens quenched at the slower rate had the faster crack growth rate. This finding agrees with data from other studies in which intergranular corrosion susceptibility was determined by measuring percent loss in tensile strength of pre-exposed sheet tension specimens.

Naval Research Laboratory

1. B. F. Brown, "Application of Fracture Mechanics and Fracture Technology to Stress-Corrosion Cracking," Presentation to ASM Conference on Fracture Control, Philadelphia, Pa., 26-28 January, and also to be presented, Houston, Texas., 10-12 March, and Chicago, Illinois, 20-22 May 1970; ASM

This paper is intended primarily to be of immediate utility to the metallurgist, the materials engineer, and the corrosionist, particularly those who are concerned with the use of high strength structural alloys in moderately corrosive environments. The paper explains why the traditional stress corrosion parameter which has been used for materials of much lower strengths can cause one to infer gross errors in order-of-merit ranking of the higher strength materials with respect to their resistance to stress-corrosion cracking. The use of fracture-mechanics type specimens is shown to obviate these errors, and analysis of the results of tests on such specimens yields not only a correct order-of-merit ranking, but also quantitative figures of merit. Test specimens and useful methods of presentation of fracture-mechanics stress-corrosion data are illustrated.

2. B. F. Brown, "Overview of the Stress-Corrosion Cracking Problem," To be presented to the ASM Conference on Stress Corrosion, Los Angeles, California, 21-23 April 1970; New Orleans, Louisiana, 2-4 June 1970; and Philadelphia, Pennsylvania, 4-6 August 1970,

The introduction includes definitions of a number of terms relating to crack propagation caused by the conjoint action of stress and corrosion and related phenomena. This is followed by a brief historical review during the course of which it becomes evident that stress-corrosion cracking, far from being restricted to a few alloys, is a general phenomenon observed in most families of alloys if the composition, heat treatment, and environment are favorable. The role of fracture mechanics in conducting and interpreting stress-corrosion cracking tests is discussed, and the several classes of mechanisms which have been postulated to account for stress-corrosion cracking are enumerated. The most serious deficiency in stress-corrosion technology is the inability to predict those combinations of alloys and environments which will give rise to stress-corrosion cracking.

E. ABSTRACTS OF RELATED ARTICLES ON STRESS-CORROSION CRACKING

1. S. Orman, "A Rapid Test For Stress-Corrosion Cracking," Corrosion Science, Vol. 9, No. 11, Nov 1969, pp. 849-851

A simple rapid test has been used to examine the susceptibility to stress-corrosion cracking (SCC) of a variety of alloys. The results are in agreement with those from longer term tests. The advantages claimed for this test are speed of assessment and the use of standard laboratory apparatus.

2. D. T. Powell and J. C. Scully, "Fractographic Observations of the Stress Corrosion Cracking of Titanium Alloys in Methanolic Environments," Corrosion, Vol. 25, No. 12, Dec 1969, pp. 483-492

The stress corrosion cracking of titanium of three different impurity levels and of Ti-5Al-2.5Sn alloy containing both low and high amounts of Fe has been examined by scanning electron microscopy. Two types of testing were employed: U-bends and dynamic tensile straining. Increasing levels of impurity resulted in a change in the mode of cracking in titanium from intergranular separation to transgranular cleavage. Both alloys exhibited transgranular cleavage. Introducing small amounts of the hydride phase in the most impure titanium resulted in (1) a larger amount of cleavage in subsequent stress corrosion tests, and (2) air fractures that were similar to stress corrosion fractures. Pre-exposure of unstressed specimens to the environment followed by fracture in air also resulted in small regions of similar fractures. Anodic dissolution superimposed on specimens during the pre-exposure period eliminated this region provided that the rate of dissolution was similar to the rate of H diffusion. A detailed discussion of the results interprets intergranular dissolution as arising mainly from impurity segregation and transgranular cleavage as being due to a form of H embrittlement.

3. V. J. Colangelo and M. S. Ferguson, "The Role of the Strain Hardening Exponent in Stress Corrosion Cracking of a High Strength Steel," Corrosion, Vol. 25, No. 12, Dec 1969, pp. 509-514

Stress corrosion testing of a vanadium modification of 4340 alloy was conducted using precracked specimens in a cantilever beam apparatus. Plastic zones at the crack tip were determined using optical interference

measurements, and the effect of these plastic zones on the fracture paths was demonstrated. Crack propagation rates were measured for steels of varying yield strengths (140-205 ksi). Electron fractographs and photomicrographs associated with the fracture through plastic zone are presented. Crack propagation rates were shown to vary inversely with the yield strength of the steel with the overall failure time being related to both the propagation rate and the fracture toughness of the material.

F. DIARY OF EVENTS

D. E. Piper presented "The Relationship Between Test Results and Service Experience," during the Symposium on the Engineering Practice to Avoid Stress Corrosion Cracking, 29th Meeting of the Structures and Materials Panel of AGARD, Istanbul, Turkey, 31 September 1969.

At the 1969 Tri-Service Meeting on Corrosion of Military Equipment, Annapolis, Md., 19-21 November 1970, B. F. Brown presented "The ARPA Coupling Program on Stress-Corrosion Cracking."

The ARPA meeting on steels was held at Carnegie-Mellon University on 27 January 1970. The meeting was very productive according to all comments from the various attendees, including those from various industries and universities outside the coupling program as well as from those within the program.

Dr. Brown presented the first of three invited lectures on "The Application of Fracture Mechanics to Stress-Corrosion Cracking," to the ASM Educational Conference on Fracture Control for Metal Structures, Philadelphia, Pa., 27 January 1970.

DOCUMENT CONTROL DATA - R&D

(Security classification of title, body of abstract and indexing annotation must be entered when the overall report is classified)

1. ORIGINATING ACTIVITY (Corporate author)
Naval Research Laboratory
Washington, D.C. 20390

2a. REPORT SECURITY CLASSIFICATION
Unclassified

2b. GROUP

3. REPORT TITLE
ARPA Coupling Program on Stress-Corrosion Cracking
(Thirteenth Quarterly Report)

4. DESCRIPTIVE NOTES (Type of report and inclusive dates)
A progress report on the problem.

5. AUTHOR(S) (Last name, first name, initial)
G. Sandoz (General Editor)

6. REPORT DATE	7a. TOTAL NO. OF PAGES	7b. NO. OF REFS
March 1970	66	37

8a. CONTRACT OR GRANT NO.	9a. ORIGINATOR'S REPORT NUMBER(S)
M04-08	NRL Memorandum Report 2101
b. PROJECT NO. RR 007-08-44-5512	
c. ARPA Order 878	9b. OTHER REPORT NO(S) (Any other numbers that may be assigned this report)
d.	

10. AVAILABILITY/LIMITATION NOTICES
This document has been approved for public release and sale; its distribution is unlimited.

11. SUPPLEMENTARY NOTES	12. SPONSORING MILITARY ACTIVITY
	Department of the Navy (Office of Naval Research), and Advanced Research Projects Agency

13. ABSTRACT

A progress report of the research investigations being carried out on the problem of stress-corrosion cracking of high strength materials under ARPA Order 878 is presented. Work at Carnegie-Mellon University, Lehigh University, Georgia Institute of Technology, The Boeing Company, American University, and the Naval Research Laboratory concerning test techniques, materials characterization, physical metallurgy, surface studies, and corrosion fatigue is described. The report is divided into three main sections covering work on high strength titanium, steel, and aluminum. Included is a section containing abstracts of recently published reports, journal articles, and talks generated under ARPA Order 878. Selected abstracts of articles from outside the ARPA program in the field of stress-corrosion cracking are also included as well as a Diary of Events section.

14. KEY WORDS	LINK A		LINK B		LINK C	
	ROLE	WT	ROLE	WT	ROLE	WT
Stress-Corrosion Cracking						
High Strength Steels						
Titanium Alloys						
Aluminum Alloys						
Electrochemistry						
Fracture Mechanics						
Surface Chemistry						